Published in final edited form as:
Neuron. 2009 January 29; 61(2): 259–271. doi:10.1016/j.neuron.2008.12.004.

Axon initial segment Ca^{2+} channels influence action potential generation and timing

Kevin J. Bender* and **Laurence O. Trussell**
Vollum Institute and Oregon Hearing Research Center, Oregon Health and Science University, Portland, OR 97239

Summary

Although action potentials are typically generated in the axon initial segment (AIS), the timing and pattern of action potentials is thought to depend on inward current originating in somatodendritic compartments. Using 2-photon imaging, we show that T- and R-type voltage-gated Ca^{2+} channels are co-localized with Na^{+} channels in the AIS of dorsal cochlear nucleus interneurons, and that activation of these Ca^{2+} channels is essential to the generation and timing of action potential bursts known as complex spikes. During complex spikes, where Na^{+}-mediated spikelets fire atop slower depolarizing conductances, selective block of AIS Ca^{2+} channels delays spike timing and raises spike threshold. Furthermore, AIS Ca^{2+} channel block can decrease the number of spikelets within a complex spike, and even block single, simple spikes. Similar results were found in cortex and cerebellum. Thus, voltage-gated Ca^{2+} channels at the site of spike initiation play a key role in generating and shaping spike bursts.

Keywords

action potential; axon initial segment; complex spike; electrophysiology; Ca^{2+} imaging; Ca^{2+} channels

Introduction

Periods of high-frequency action potential discharges, termed bursts, are a mechanism for encoding neural information within spike trains. Burst firing is an integral component of a variety of neural computations, including sensory processing, attention, circuit-wide oscillations in activity rates, and synaptic plasticity (reviewed in: Krahe and Gabbiani, 2004; Lisman, 1997). Action potentials within bursts often fire atop long-lasting depolarizations. Present evidence suggests that these long depolarizations are generated exclusively by intrinsic and synaptic conductances in somatodendritic compartments. These slow waveforms then trigger action potential generation in the proximal part of the axon, the axon initial segment (AIS) (Bean, 2007).

The AIS is a specialized cellular compartment that has been identified as the site of action potential initiation in a wide variety of cells (Coombs et al., 1957; Goldberg et al., 2008; Khaliq and Raman, 2006; Mainen et al., 1995; Martina et al., 2000; Palmer and Stuart, 2006; Shu et

*Correspondence: benderke@ohsu.edu.

al., 2007; Stuart et al., 1997). It is characterized by a high density of Na^+ channels anchored to a thick cytoskeleton network (Catterall, 1981; Kole et al., 2008; Palay et al., 1968; Wollner and Catterall, 1986). Recent studies indicate that the AIS is also enriched with K^+ channels, and that the availability of Na^+ and K^+ conductances in the AIS depends on recent activity (Goldberg et al., 2008; Kole et al., 2007). While the presence of these channels clearly facilitates generation of individual fast spikes in axons, it remains unclear what ionic mechanisms exist that allow somatically triggered spike bursts to invade axons and lead to a reliable and potent cluster of synaptic signals.

We examined initial segment Ca^{2+} signals in cartwheel cells, Purkinje-like interneurons found in the dorsal cochlear nucleus, a cerebellum-like auditory brainstem nucleus (Oertel and Young, 2004). A particular advantage of cartwheel cells as a model preparation is that their local, compact axonal arbor allows one to image Ca^{2+} in all compartments, from dendritic spine to axonal bouton. Cartwheel cells fire both Na^+-mediated simple spikes and complex spikes, a form of burst firing where Na^+-dependent action potentials termed spikelets ride on slower, Ca^{2+} depolarizations (Kim and Trussell, 2007; Molitor and Manis, 2003; Schmolesky et al., 2002). Spike timing in cartwheel cells plays a key role in triggering synaptic plasticity (Tzounopoulos et al., 2004). Their complex spikes can be evoked by somatic depolarization, allowing a high level of experimental control over complex spike patterns. Using Ca^{2+} and Na^+ imaging, we found that T- and R-type voltage-gated Ca^{2+} channels were present in the AIS. Ca^{2+} channels were co-distributed with Na^+ channels, and served to boost membrane depolarization over the entire time course of a complex spike. Moreover, activation of AIS Ca^{2+} channels determined both the probability of spiking and spike timing. Similar results were found in cortical layer 5b pyramidal cells and cerebellar Purkinje cells, suggesting that this is a common feature of bursting cells. Thus, these data support a model in which AIS Ca^{2+} currents modify somatodendritic excitatory signals and thereby provide the final determination of the properties of a spike burst.

Results

Na^+ and Ca^{2+} signals in cartwheel cells

We performed whole-cell recordings from cartwheel cells in mouse dorsal cochlear nucleus and assayed spike-evoked Na^+ and Ca^{2+} transients in various cellular compartments using 2-photon laser scanning microscopy. Previous studies show that cartwheel cells have a typical AIS, with an electron dense plasma membrane undercoating, fascicles of microtubules, and a myelin sheath that does not form until 30–35 μm from the hillock (Wouterlood and Mugnaini, 1984). A hallmark of the AIS in other cells is a high density of Na^+ channels (Catterall, 1981; Wollner and Catterall, 1986). Studies in pyramidal and Purkinje neurons utilizing low-affinity Na^+ dyes have shown that spike-triggered Na^+ transients are largest in the AIS, with little to no signal observed in other cellular compartments (Kole et al., 2008; Lasser-Ross and Ross, 1992). Here, we recorded from cartwheel cells with patch pipettes loaded with the volume marker Alexa 594 and the Na^+ indicator CoroNa. Cell morphology was assessed by visualizing Alexa 594 after the two dyes filled the neuron (see Methods; Fig. 1A). Linescans were made in various cellular structures, and Na^+ transients were measured in response to a train of 12 simple spikes at 100 Hz (Fig. 1B). Large Na^+ signals were observed in the first 25–30 μm of axon, consistent with the presence of a high density of Na^+ channels in the AIS. Little to no Na^+ signal was detected in the soma, dendrites, or axonal boutons (Fig. 1C–D). Because the complex spike of cartwheel cells is driven by a Ca^{2+} dependent voltage waveform (Kim and Trussell, 2007; Molitor and Manis, 2003; Schmolesky et al., 2002), we next asked if voltage-gated Ca^{2+} channels might also concentrate in the AIS. To test this, we replaced CoroNa with the Ca^{2+} indicator Fluo-5F (Fig. 2). Trains of simple spikes evoked Ca^{2+} transients in cartwheel cell dendrites and axonal boutons, consistent with previous results (Roberts et al., 2008).

Surprisingly, Ca^{2+} transients in the proximal axon were as large as those observed in boutons and dendrites, and appeared to be strictly confined to the AIS (peak train ΔG/R, AIS: 6.16 ± 0.52%, n = 26 sites, 7 cells; bouton: 6.07 ± 0.85%, n = 8 boutons, 4 cells; dendrite: 6.50 ± 0.33%, n = 16 sites, 6 cells). Similar relationships were observed when only single spikes were used to evoke Ca^{2+} transients (Fig. 2D; peak single spike ΔG/R, AIS: 1.86 ± 0.16%, bouton: 1.60 ± 0.39%, dendrite: 1.00 ± 0.38%). ΔG/R values in the AIS correspond to $[Ca^{2+}]$ elevations of 1.1 to 3.6 μM for single spikes and trains, respectively.

To determine if Na^+ and Ca^{2+} signals were co-distributed in the AIS, we performed simultaneous Na^+ and Ca^{2+} imaging in mice expressing GFP in cartwheel cells (Fig. 3A, Oliva et al., 2000;Roberts et al., 2008). Cells with intact axons were identified using GFP and patched with an internal solution containing CoroNa and a red Ca^{2+} indicator, X-rhod-5F. A linescan site was selected while imaging GFP using 970 nm light, and then the laser was re-tuned to 770 nm. Both CoroNa and X-rhod-5F were easily excited at this wavelength, but GFP was not (see Methods). Thus, we were able to separately assay morphology or Na^+ on the same green channel by changing the excitation wavelength. Trains of 12 simple spikes at 100 Hz elicited both Ca^{2+} and Na^+ transients (Fig. 3B). Linescans were made in the soma, dendrite, and along the first 40 μm of the axon (n = 7 cells, 4–11 linescans/5 μm bin). When CoroNa and X-rhod-5F signals were scaled to their respective maxima, we found that Ca^{2+} and Na^+ signals covaried >10 μm from the axon hillock (Fig. 3C). Further, point by point comparisons of Na^+ and Ca^{2+} signals across all axonal imaging sites were correlated positively (Fig. 3D; n = 39 sites, 4 cells, $R^2 = 0.4$, $p < 0.0001$, linear regression). As in experiments examining Ca^{2+} or Na^+ alone, Ca^{2+} transients in the dendrites were as large as those found in the AIS, but Na^+ signals were near zero (Fig. 3C, n = 7 sites), suggesting that the indicators used were selective for their respective ion.

While Ca^{2+} and Na^+ signals co-varied in the distal AIS, Ca^{2+} transients were larger within the first 10 μm of the axon and in the soma (Fig. 3C). This could reflect a higher relative density of Ca^{2+} channels in the early portion of the AIS, or be due to diffusion of either Ca^{2+} or Ca^{2+}-bound dye from the somatodendritic domain. To test the latter, we isolated the Ca^{2+}-mediated component of complex spikes by blocking Na^+ channels with tetrodotoxin (TTX, Fig. 4). The resulting depolarizations yield large somatodendritic Ca^{2+} transients (Molitor and Manis, 2003). Under these conditions, Ca^{2+} signals were observed only within the first 10 μm of axon, and their amplitude fell exponentially with distance from the hillock (Fig. 4B–D, length constant: 3.9 ± 0.2 μm, n = 5 cells), consistent with diffusion of Ca^{2+} or Ca^{2+}-bound dye, or passive depolarization of the most proximal part of the AIS that in turn opened voltage-gated Ca^{2+} channels. These data also suggest that the distal AIS was electrically isolated from the somatodendritic domain, and that Ca^{2+} channels in this region required local depolarization through Na^+ channels for activation.

The AIS contains T- and R-type Ca^{2+} channels

To identify the Ca^{2+} channel classes mediating Ca^{2+} influx in the AIS, we examined Ca^{2+} transients resulting from trains of simple spikes in the presence of various Ca^{2+} channel antagonists (Fig. 4). Linescans were made 15.7 ± 0.2 μm from the axon hillock to minimize non-axonal Ca^{2+} sources (see Fig. 4). Ca^{2+} transients were reduced to 41.9 ± 2.6% of baseline levels by 3 μM mibefradil, a T-type Ca^{2+} channel antagonist (Fig. 5A, E; n = 5 cells, $p < 0.0001$, one sample t-test). Transients were further reduced by the R-type blocker SNX-482 (Fig. 5B, E; 500 nM; SNX-482 alone: 79.7 ± 3.3%, n = 3, $p < 0.05$; SNX-482 + mibefradil: 11.0 ± 3.9%, n = 4, $p < 0.001$, one sample t-test). Low concentrations of Ni^{2+} (50 μM), specific for R- and T-type channels (Kampa et al., 2006;Magee and Johnston, 1995), reduced transients to 44.3 ± 5.8% of baseline (n = 4, $p < 0.01$, one sample t-test). L- and N-type blockers had no effect on AIS Ca^{2+} (10 μM nifedipine: 100.4 ± 3.9%, n = 5, p = 0.9; 3 μM ω-conotoxin-GVIA: 100.3 ±

2.2%, n = 4, p = 0.9, one sample t-test). ω-agatoxin-TK (150 nM), a potent P/Q-channel blocker, largely blocked Ca^{2+} transients in boutons (Fig. 5C, E; 10.6 ± 3.2%, n = 6 boutons, 4 cells, p < 0.0001, one sample t-test). AIS Ca^{2+} transients were larger in agatoxin (115.2 ± 3.2%, n = 5 cells, p < 0.01, one sample t-test) and spike decay was slightly slower, probably reflecting indirect block of BK channels that repolarize spikes (Berkefeld et al., 2006). No alterations in spike shape were observed with other antagonists. Similar reductions in Ca^{2+} signals were observed when only one simple spike was used (% of control signals: mibefradil: 39.2 ± 5.7%, n = 5, p < 0.001; SNX-482: 76.4 ± 6.2%, n = 3, p = 0.06; SNX-482 + mibefradil: 11.4 ± 2.1%, n = 4, p < 0.001; Ni2+: 42.8 ± 7.3%, n = 4, p <0.01; nifedipine: 99.1 ± 2.5%, n = 5, p = 0.7; ω-conotoxin-GVIA: 103 ± 7.5%, n = 4, p = 0.7; ω-agatoxin-TK: 126.6 ± 13.9%, n = 5, p = 0.12, one sample t-test). Thus, AIS Ca^{2+} influx was mediated by a mix of T- and R-type Ca^{2+} channels, and one spike was sufficient to drive Ca^{2+} influx.

To confirm the presence of T-type Ca^{2+} channels in the AIS, we made voltage-clamp recordings and isolated T-channel currents with voltage steps from −100 to −60 mV while imaging AIS Ca^{2+} (Fig. 5D). Ca^{2+} signals rose rapidly in response to a transient T-channel current, and then continued to rise more slowly for the duration of the voltage step (I_T transient: −113 ± 30 pA, $\tau_{activation}$: 1.85 ± 0.20 ms, peak ΔG/R: 3.6 ± 0.8%, n = 5 cells), suggesting that T-channels were tonically active at −60 mV, though the tonic current was masked by outward leak currents.

Impact of AIS Ca^{2+} on complex spikes

The fact that subtle changes in spike repolarization in the presence of ω-agatoxin altered Ca^{2+} levels in the AIS suggests that the slow depolarization underlying complex spikes could significantly influence AIS Ca^{2+} levels during bursts. The depolarizing boost provided by this Ca^{2+} could in turn influence the timing or generation of spikelets riding atop the slow depolarization. To determine whether Ca^{2+} channels were activated during the entire complex spike, or only during strong, spikelet-mediated depolarizations, we compared the amount of Ca^{2+} observed in the AIS during a complex spike to what would be expected from a burst of simple spikes at the same timing. In presynaptic boutons, invading action potentials typically drive uniform increases in local Ca^{2+}, and Ca^{2+} transients resulting from bursts of action potentials can be predicted reliably by the linear sum of individual events offset by their relative timing (Brenowitz and Regehr, 2007; Koester and Johnston, 2005; Koester and Sakmann, 2000; Roberts et al., 2008; Bischofberger et al., 2002; Geiger and Jonas, 2000). We found that for trains of simple spikes (6 at 50 Hz), this relationship held true both in cartwheel cell boutons (Fig. 6A, E; observed/expected Ca^{2+} transient: 1.02 ± 0.02, n = 8 boutons, 4 cells, p = 0.35, one sample t-test), and in the AIS [Fig. 6B, E; 1.01 ± 0.01, n = 26 sites (0–22 μm from hillock), 7 cells, p = 0.33, one sample t-test]; however, complex spikes resulted in larger AIS Ca^{2+} transients than would be expected by the simple linear sum of Ca^{2+} from its constituent spikelets (Fig. 6C, E; 1.35 ± 0.05, n = 26 sites, p < 0.0001, one sample t-test). The presence of a larger-than-predicted Ca^{2+} signal indicates that Ca^{2+} influx must have occurred both during and between spikes. The latter probably reflected channel activity associated with the slow depolarization that drives spikelet generation. This supralinear Ca^{2+} level was relatively constant throughout the AIS (Fig. 6E), but returned to unity in boutons (Fig. 6D–E; 0.99 ± 0.01, n = 8, p = 0.35, one sample t-test), suggesting that all spikelets were transformed into separate propagating action potentials(Roberts et al., 2008). Observed/predicted Ca^{2+} values were not calculated for axonal sites between the AIS and boutons due to the low signal/noise of single spike responses in that area. Complex spikes also evoked supralinear Ca^{2+} transients in cartwheel cell dendrites (Fig. 6E train: 0.98 ± 0.01, p = 0.06; complex spike: 1.32 ± 0.04, p < 0.0001, n = 16 sites, 6 cells, one sample t-test), consistent with findings from a study of burst firing in cortical pyramidal cells (Kampa and Stuart, 2006).

These results indicate that the depolarization underlying a complex spike is sufficient to activate AIS Ca^{2+} channels. To determine the role of these channels during complex spikes, we blocked AIS T-type channels with a local puff of mibefradil immediately before eliciting a complex spike with 2–3 spikelets. Since complex spike dynamics change over the course of a whole-cell recording (Kim and Trussell, 2007), control complex spikes were interleaved with complex spikes paired with mibefradil puffs (mib-CS; 2s between complex spikes, then a 45s delay to allow for mibefradil wash-out). SNX-482 was not included since it does not wash out over these time scales. Mibefradil was dissolved in a HEPES-based vehicle and loaded into one side of a theta (double-barrel) pipette. The other side was loaded only with the vehicle, and the assembly was connected to a Picospritzer allowing independent control of either barrel of the pipette. Neurons with axons well separated from their dendritic field were selected and the puff pipette was placed within 2 μm of the axon, 10–12 μm from the hillock (Fig. 7A).

We found that T-type channel block principally affected two properties of complex spikes activated by a current step: spikelet timing and spikelet threshold. We calculated changes by comparing relative spikelet timing or threshold membrane voltage across pairs of control and mib-CSs (>10 trials/cell, n = 5 cells). Spikelet peaks were delayed by mibefradil, with later spikelets exhibiting greater delays (Fig. 7B, E; 1^{st} spikelet: 1.45 ± 0.30 ms, 2^{nd}: 2.36 ± 0.50, 3^{rd}: 3.30 ± 0.66; $p < 0.001$, ANOVA vs. vehicle puff). These changes in spikelet timing and inter-spikelet interval resulted from changes in spikelet threshold, as mibefradil increased the amount of depolarization required to reach threshold (Fig. 7D, F; 1^{st} spikelet: 4.46 ± 1.12 mV, 2^{nd}: 2.48 ± 1.62; $p < 0.001$) and delayed threshold onset (Supplemental Fig. 1; 1^{st} spikelet: 1.44 ± 0.29 ms, 2^{nd}: 1.92 ± 0.41; $p < 0.001$). To test whether these changes were due to specific effects of mibefradil on the AIS, we moved the puff pipette next to a proximal dendrite, ~10 μm from its somatic origin. Mibefradil puffs onto the proximal dendrite had no effect on complex spikes (Fig. 7C, E–F; timing, 1^{st} spikelet: −0.01 ± 0.04 ms, 2^{nd}: −0.05 ± 0.02, 3^{rd}: −0.15 ± 0.003, $p > 0.05$; threshold V_m, 1st spikelet: 0.03 ± 0.03 mV, 2nd: 0.18 ± 0.13, $p > 0.05$, ANOVA). Therefore, the changes in spikelet dynamics resulted from a block of AIS T-type channels.

Mibefradil puffs moved the tissue close to the pipette, making it difficult to simultaneously image Ca^{2+} transients in the AIS. We therefore employed a complementary technique to determine the extent to which AIS Ca^{2+} signaling was reduced with local Ca^{2+} channel blockade. A microelectrode containing Ni^{2+} was placed next to the axon. Control complex spikes were then interleaved with complex spikes paired with Ni^{2+} iontophoretic pulses. The iontophoretic current was adjusted to approximate the changes in spikelet timing observed with mibefradil. As in mibefradil puff experiments, both spikelet timing and spikelet threshold were altered (Fig. 8A, C–D; timing, 1^{st} spikelet: 1.63 ± 0.25 ms, 2^{nd}: 2.84 ± 0.49, 3^{rd}: 3.81 ± 0.95; threshold V_m, 1st spikelet: 4.02 ± 0.88 mV, 2^{nd}: 3.40 ± 0.51; n = 9–11 spikelets/group, 11 cells, $p < 0.001$ for all groups, one sample t-test). We imaged the axon directly adjacent to the iontophoretic pipette and found that complex spike-evoked Ca^{2+} transients were reduced to 51.2 ± 2.4% of baseline levels in Ni^{2+} (n = 9, $p < 0.0001$, one sample t-test); however, it was unclear what proportion of this decrease was due to the increase in inter-spike intervals and concomitant reduction in Ca^{2+} transient summation (Fig. 8B, E). To evaluate changes in Ca^{2+} signaling independent of changes in spike timing, we replaced complex spikes with trains of 6 simple spikes at 50 Hz while maintaining the timing and intensity of the iontophoretic pulse. Train-evoked Ca^{2+} transients were reduced to 53.0 ± 4.1% of baseline in the AIS (Fig. 8B, E; n = 10, $p < 0.0001$, one sample t-test), suggesting that reductions observed with complex spikes were primarily due to Ca^{2+} channel block. The effective concentration of Ni^{2+} during these experiments was under 50 μM, as local block reduced Ca^{2+} transients less than bath application of 50 μM Ni^{2+} (Fig. 5E). We next performed linescans through the soma and a proximal dendrite and found that Ca^{2+} signals were not altered by the application of Ni^{2+} to the AIS (Fig. 8B, E; soma: 100.4 ± 1.9% of control, n = 10, p = 0.8; dendrite: 100.7 ± 1.4%,

n = 10, p = 0.6, one sample t-test). Combined with mibefradil puff experiments, these results suggest that Ca^{2+} channel block was localized to the AIS, and that the changes in spike timing and threshold were due to a ~50% reduction in local Ca^{2+}.

AIS Ca^{2+} current regulates spike generation

Since spike threshold is more depolarized when AIS T-type channels are blocked, it is likely that T-type channel activation can gate spike generation from what would otherwise be a subthreshold stimulus. In a subset of Ni^{2+} iontophoretic experiments, we substituted EPSP-like somatic current injections for square waves to better mimic parallel fiber activity. EPSP-like stimuli were based on recorded parallel fiber EPSPs, and allowed us to depolarize the AIS in a controlled, highly repeatable fashion (Roberts et al., 2008). Stimulus amplitude was first adjusted to just suprathreshold levels for a single, simple spike. When paired with Ni^{2+}, spikes were blocked (Fig. 9A–B; control spikes/stim: 1.00 ± 0.00, Ni^{2+}: 0.06 ± 0.06; $p < 0.03$, Wilcoxon signed rank test, n = 6 cells). We then increased the stimulus amplitude to elicit complex spikes with 2–3 spikelets. Again, Ni^{2+} reduced the number of spikelets evoked with each stimulus (Fig. 9A, C; control: 2.11 ± 0.12, Ni^{2+}: 1.24 ± 0.13; $p < 0.01$, Wilcoxon signed rank test, n = 9 cells).

To determine how quickly Ca^{2+} channels were activated with these stimuli, we examined the timecourse of subthreshold depolarization in control and Ni^{2+}-paired conditions where single spikes were blocked by Ni^{2+}. The average difference between conditions was calculated for each cell (Ctrl-Ni^{2+}: Fig. 9D). Differences between control and Ni^{2+}-paired depolarizations were evident within 0.77 ± 0.07 ms of stimulus onset (Fig. 9D–F; n = 6 cells). By the time spike threshold was reached in control conditions, Ni^{2+}-paired depolarizations were reduced 4.8 ± 0.4 mV (measured for each sweep; n = 46 sweeps, 6 cells). Therefore, AIS Ca^{2+} channels not only influence spikelet timing within complex spikes, they can also provide depolarization necessary for spike generation, and do so within 1 ms of stimulus onset.

Does AIS Ca^{2+} drive Ca^{2+}-activated K^+ channels?

In addition to contributing to local depolarization, Ca^{2+} can activate big and small conductance K^+ channels, BK and SK. While both SK and BK are expressed in cartwheel cells (Kim and Trussell, 2007), it is unclear whether they co-localize with Ca^{2+} channels in the AIS. To test this, we first examined aspects of complex spike waveforms that could change if Ca^{2+} channel block by mibefradil or Ni^{2+} were also indirectly blocking BK/SK signaling. Block of BK channels by bath application of iberiotoxin (IbTX) slows spike repolarization rates in cartwheel cells (Kim and Trussell, 2007); however, repolarization rates were not altered by AIS Ca^{2+} block with mibefradil or Ni^{2+} (Supplemental Fig. 1). During complex spikes, bath application of IbTX or the SK antagonist apamin depolarizes inter-spikelet repolarization potentials (Kim and Trussell, 2007). As with spike repolarization rates, inter-spikelet repolarization was not affected by AIS Ca^{2+} channel block (Supplemental Fig. 1); however, this could reflect a balance between reductions in both Ca^{2+} influx and K^+ efflux with the block of Ca^{2+} and BK/SK channels, resulting in no net change in repolarization potential. Therefore, we repeated local Ni^{2+} iontophoresis experiments, but blocked SK and BK by bath application of 100 nM apamin and 100 nM IbTX, respectively. If AIS Ca^{2+} activated BK and SK channels, these conditions should reveal the isolated contribution of reduced Ca^{2+} influx to inter-spikelet repolarization potential. Bath application of apamin and IbTX produced characteristic changes to action potentials evoked with long step somatic current injections (Supplemental Fig. 2A, C). Complex spikes with 2–3 spikelets could still be evoked with short step currents, and when paired with AIS Ni^{2+} iontophoresis, spikelet timing was delayed (Supplemental Fig. 2B, D–E; e.g., 1st spikelet delay: 1.80 ± 0.30 ms in apamin, n = 8; 2.14 ± 0.41 ms in IbTX, n = 7; $p > 0.2$ for all conditions vs. Ni^{2+} iontophoresis alone, unpaired t-test), but inter-spikelet repolarization potentials were not altered (Supplemental Fig. 2B, D, F; e.g., relative

repolarization following 1st spikelet: 0.11 ± 0.19 mV in apamin, n = 8; 0.57 ± 0.26 mV in IbTX, n = 7; mV, n = 11 for Ni^{2+} iontophoresis alone; p > 0.3 vs. apamin and IbTX, unpaired t-test). Thus, AIS Ca^{2+} did not appear to drive local BK or SK activity in a way that significantly altered simple or complex spike initiation.

Bursts in other bursting cell types are also shaped by AIS Ca^{2+} channels

Spike bursts are common to many cell types. To determine if AIS Ca^{2+} channels have a general role in regulating bursts, we replicated key aspects of this study in two other cell types from other, non-auditory brain regions: primary somatosensory cortex layer 5b pyramidal cells, and cerebellar Purkinje cells (Fig. 10A). Similar to cartwheel cells, both pyramidal and Purkinje cell action potentials initiate in the axon (Davie et al., 2008;Khaliq and Raman, 2006;Palmer and Stuart, 2006), and spike bursts drive elevations in dendritic Ca^{2+} (Kampa and Stuart, 2006;Sugimori and Llinas, 1990). Ca^{2+} transients in response to trains of action potentials (6 × 50 Hz) were observed in the AIS of both cells (Fig. 10B, Pyramidal: ΔG/R: 5.39 ± 0.99%, recorded 15.2 ± 1.4 μm from axon hillock, n = 6 cells; Purkinje: ΔG/R: 4.89 ± 0.73%, 16.3 ± 1.8 μm from hillock, n = 5 cells). These Ca^{2+} transients could be reduced to 53 ± 6% and 53 ± 5% of baseline when trains were paired with local Ni^{2+} iontophoresis in pyramidal and Purkinje cells, respectively (n = 5 for both cell types). As in cartwheel cells, pairing Ni^{2+} iontophoresis with spike bursts (2–3 spikes/burst) raised spike threshold and delayed spike timing (Fig. 10C–E; Pyramidal cell: relative spike timing delay, 1st spike: 2.07 ± 0.39 ms, p < 0.01; 2nd spike: 3.48 ± 0.60 ms, p < 0.001; relative threshold depolarization, 1st spike: 2.86 ± 0.37 mV, p < 0.001; 2nd spike: 2.63 ± 0.41 mV, p < 0.001, n = 8 cells; Purkinje cell: relative spike timing delay, 1st spike: 0.86 ± 0.12 ms, p < 0.001; 2nd spike: 1.49 ± 0.28 ms, p < 0.01; relative threshold depolarization, 1st spike: 2.77 ± 0.80 mV, p < 0.05; 2nd spike: 3.26 ± 1.08 mV, p < 0.05, n = 6 cells, one sample t-test). In pyramidal cells, we found that this effect was specific to AIS Ca^{2+} channel block; Ni^{2+} iontophoresis onto neighboring basal dendrites had no effect on the timing of spikes within bursts (relative spike timing, 1st spike: 0.05 ± 0.10 ms; 2nd spike: −0.15 ± 0.17 ms; relative threshold, 1st spike: −0.15 ± 0.16 mV, 2nd spike −0.18 ± 0.19 mV; p > 0.4 for all conditions, one sample t-test; dendrites were 20 ± 4 μm from axon, n = 4 dendrites, 2 cells). Thus, initial segment Ca^{2+} channels have similar roles in both excitatory and inhibitory cell types found in diverse brain regions.

Discussion

These results show that voltage-gated Ca^{2+} channels localized to the initial segment have a substantial impact on the timing and generation of action potentials. We estimate that Ca^{2+} transients during activity reflected a 1.1 to 3.2 μM increase in local Ca^{2+} with single and complex spikes, respectively, and that Ca^{2+} current contributed substantially to local membrane depolarization. When Ca^{2+} channels were blocked with T- and R-type channel antagonists, spike timing within bursts was delayed, threshold was elevated, and spike probability dropped. Since Ca^{2+} levels were reduced by only ~50% while localizing pharmacological effects to the AIS, the overall impact of AIS Ca^{2+} channels could be larger than that reported here.

This work suggests that the initial segment is the site of action potential initiation in cartwheel cells, as Na^{+} channels were concentrated there and because manipulations of AIS Ca^{2+} affect both single and complex spikes. This conclusion is consistent with recent work in cerebellar Purkinje cells indicating that all complex spike spikelets originate in the axon (Davie et al., 2008). Experimental and theoretical data suggest that the AIS—and in some cases, the distal end of the AIS—is the site of action potential generation (Khaliq and Raman, 2006; Mainen et al., 1995; Palmer and Stuart, 2006); therefore, currents present there have the greatest influence on spike initiation. We found Ca^{2+} transients throughout the AIS, including the distal

end (Figs. 2–3). Ca^{2+} transients during complex spikes exceeded those expected from the simple sum of Ca^{2+} entry from the same number of similarly timed simple spikes by at least 35%, suggesting that AIS Ca^{2+} channels were sensitive to subthreshold depolarizations such as the underlying component of complex spikes. This likely underestimates the relative contribution of the underlying complex spike depolarization to total AIS Ca^{2+}, since later spikelets within complex spikes were not as large as the simple spikes used to generate estimates. Thus, subthreshold depolarizations have a significant influence on action potential initiation through activation of AIS Ca^{2+} channels.

Recent work in cortical pyramidal cells has shown that AIS Na^+ channels mediate local subthreshold depolarizations that precede action potential initiation (Kole and Stuart, 2008). Here, we found that blocking Na^+ channels with TTX had a profound effect on AIS Ca^{2+} channel signaling. In TTX, the Ca^{2+}-mediated component of complex spikes could still be observed in the somatodendritic domain, but Ca^{2+} transient amplitude in the AIS fell exponentially with distance from the hillock (Fig. 4). This suggests that without subthreshold Na^+ channel activity, the AIS is electrotonically isolated from the somatodendritic domain. AIS Ca^{2+} channels therefore may require subthreshold Na^+ current for activation, and thus the two may act in synergy to drive membrane potential to action potential threshold. What remains unclear is whether this synergistic action not only promotes generates of spikelets in the AIS but also the conduction of full amplitude, propagating spikes in the axon (Roberts et al., 2008).

Properties of initial segment Ca^{2+} channels

In cartwheel cells, AIS Ca^{2+} transients were reduced by mibefradil, Ni^{2+}, and SNX-482, but not by nifedipine, conotoxin, or ω-agatoxin (Figs. 5, 7–8), suggesting that the AIS contains only R- and T-type Ca^{2+} channels. SNX-482, a selective antagonist of α_{1E}-containing R-type ($Ca_v2.3$) channels, blocked ~20% of the local Ca^{2+} signal. Ca^{2+} transients were further reduced with bath application of mibefradil, which is most selective for T-type channels ($Ca_v3.X$) (McDonough and Bean, 1998), but can also block R-type channels at low concentrations and other voltage gated channel types at higher concentrations (Perez-Reyes, 2003). To confirm the presence of low-voltage activated T-channels, we made voltage steps to only −60 mV, a stimulus which evoked both a transient inward current and a Ca^{2+} signal in the AIS. Co-application of mibefradil and SNX-482 did not block AIS Ca^{2+} transients completely. This small, residual Ca^{2+} transient could arise from several sources, including toxin-insensitive R-type channels (Metz et al., 2005;Tottene et al., 2000) or diffusion of Ca^{2+} or Ca^{2+}-bound dye from the soma (Fig. 4).

Both bath application of 50 μM Ni^{2+} and local Ni^{2+} iontophoresis reduced AIS Ca^{2+} transients by ~50% in cartwheel cells. Given that similar reductions were observed with Ni^{2+} iontophoresis in pyramidal and Purkinje cells, and that Ni^{2+} is relatively specific for T- and R-type Ca^{2+} channels at this concentration (Magee and Johnston, 1995), these channel subtypes are likely present in the AIS of these other cell types. Direct pharmacological analysis will be required to determine whether other Ca^{2+} channel subtypes are present in the AIS of pyramidal and Purkinje cells.

A major feature of T-type channels is that while they activate quickly, they inactivate rather slowly, providing an ideal mechanism to exert control over relatively long duration events like spike bursts. By analyzing the kinetics of subthreshold depolarizations in the presence of local Ni^{2+}, we found that Ca^{2+} channels activated within 1 ms of stimulus onset, and boosted somatically recorded membrane potential ~5 mV by spike onset (Fig. 9). This initial current was likely mediated by either $Ca_v3.1$ or 3.2 channels. Activation kinetics of T-channel currents isolated by voltage-clamp steps from −100 to −60 mV were similar to those isolated in HEK cells (Lee et al., 1999). Later current could incorporate $Ca_v3.3$ channels, which are slower to

activate, and $Ca_v2.3$ R-type channels, which require more depolarization to open (Catterall et al., 2005).

The largest effects of AIS Ca^{2+} channel block were on the timing and threshold of spikes triggered by current steps, which could be due to changes in the rate and amplitude of membrane depolarization, or Ca^{2+}-dependent modifications of local Na^+ channels. Calmodulin-regulated $Na_v1.6$ channels are expressed in the AIS (Boiko et al., 2003); however, Ca^{2+} alters their inactivation rates, not threshold or activation rates (Herzog et al., 2003). AIS Ca^{2+} did not appear to activate BK or SK channel. BK channels typically co-localize with P/Q channels (Berkefeld et al., 2006), which were not present in the AIS (Fig. 4), and have dramatic effects on spike repolarization rates, which were not altered with local mibefradil or Ni^{2+} application (Supplemental Fig. 1). SK channels, which help shape inter-spike repolarizations, are often linked to T-type Ca^{2+} channels (Cueni et al., 2008; Wolfart and Roeper, 2002), but inter-spike repolarization levels were not altered by SK or BK antagonists (Supplemental Fig. 2). Therefore, we suggest that initial segment Ca^{2+} channels largely provide a depolarizing drive, but it remains unknown whether AIS Ca^{2+} drives any second messenger pathways, at these or other timescales.

Ca^{2+} channels are not typically thought to be concentrated in the initial segment, and while immunohistochemistry suggests that T-type channels are expressed in axon, signal levels are too weak to draw a definitive conclusion (McKay et al., 2006). T- and R- channel histology rarely shows labeling beyond the soma and proximal dendrites, suggesting that current antibodies are not sensitive enough to identify channels throughout all neural arbors (Day et al., 1996). In contrast, Ca^{2+} imaging techniques readily detect Ca^{2+} influx through pharmacologically identified low-threshold channels throughout dendritic trees (Goldberg et al., 2004), and axonal Ca^{2+} transients have been shown in a variety of neurons, including cerebellar Purkinje, cortical pyramidal—both in this report and in others—and dorsal root ganglion cells (Callewaert et al., 1996; Luscher et al., 1996; Schiller et al., 1995). Indeed, Ca^{2+} imaging combined with channel pharmacology might provide a more accurate assessment of Ca^{2+} channel localization than currently available Ca^{2+} channel antibodies.

Bath application of R- and T-channel antagonists alters spike threshold in cartwheel cells, reduces the number of spikelets in cartwheel and cerebellar Purkinje cells, and can even prevent complex spike initiation at the onset of step depolarizations (Cavelier et al., 2008; Kim and Trussell, 2007). We obtained similar results while only blocking AIS Ca^{2+} channels. This suggests that some results previously attributed to somatodendritic Ca^{2+} channels might be mediated at least in part by Ca^{2+} channels in the initial segment. For example, cells of the cerebellar nuclei fire characteristic rebound bursts following strong hyperpolarizations, a phenomenon known to require T-type channels (Aizenman and Linden, 2000). AIS T-type channels in close proximity to the spike initiation zone would be ideally suited to drive this rebound firing. Furthermore, while we have shown that AIS Ca^{2+} is important for other cells that fire bursts (Fig. 10), they could also play important roles in cells that have Ca^{2+}-mediated after depolarizations, or Ca^{2+} channel-mediated oscillations (Bean, 2007; Cueni et al., 2008; Metz et al., 2005). Careful dissection of AIS and somatodendritic Ca^{2+} channel contributions would be required to determine if this is the case in these cell types.

Functional implications for bursting cells

An intriguing aspect of these results is that the AIS incorporates low-threshold Ca^{2+} channels that are selectively recruited from more hyperpolarized membrane potentials. Cartwheel cells operate over a broad range of resting membrane potentials, and can be quiescent or spontaneously active *in vitro* and *in vivo* (Davis and Young, 1997; Kim and Trussell, 2007). Complex spikes are evoked preferentially at the onset of long current steps only when the basal membrane potential is well hyperpolarized, presumably reflecting the availability of low

threshold T-channels (Kim and Trussell, 2007). Further, T-channel-dependent complex spikes evoked from hyperpolarized membrane potentials tend to have more spikelets with shorter inter-spikelet intervals compared to complex spikes evoked from depolarized levels (Kim and Trussell, 2007). Similarly, bursts in many cell types, including thalamic relay and pyramidal cells, vary based on recent membrane potential and spiking activity (Destexhe et al., 1998; Williams and Stuart, 1999). Thus, Ca^{2+} channels localized to the initial segment could help encode the recent voltage history of a neuron in the patterns within spike bursts and have a significant impact on information processing and synaptic plasticity (Harris et al., 2001; Krahe and Gabbiani, 2004; Lisman, 1997; Magee and Johnston, 1997).

Experimental procedures

Electrophysiology

All procedures were conducted in accordance with OHSU IACUC guidelines. Following anesthesia, coronal brainstem slices (210 μm) were made from P17-21 ICR (Harlan, Indianapolis, IN) mice or GIN mice expressing GFP in cartwheel cells. GIN mice were phenotyped as described previously (Roberts et al., 2008). Cutting solution contained (in mM): 130 NaCl, 3 KCl, 2.4 $CaCl_2$, 1.3 $MgSO_4$, 1.2 KH_2PO_4, 20 $NaHCO_3$, 3 Na-HEPES, 10 glucose; bubbled with 5%CO_2/95%O_2; ~305 mOsm, 33–34 °C. Following cutting, slices were incubated for 1 hr at 33 °C, then at room temperature until recording. Cartwheel cells were identified based on their dendritic morphology and their ability to fire complex spikes in response to somatic depolarization (Wouterlood and Mugnaini, 1984; Zhang and Oertel, 1993). Recordings were made at 33 °C. For recording, $CaCl_2$ was reduced to 1.0 mM and $MgSO_4$ was raised to 2.7 mM to maintain the divalent concentration, unless otherwise noted. This Ca^{2+} concentration is lower than used previously (Roberts et al., 2008), and may account for more reliable spikelet propagation. DNQX (10 μM), strychnine (500 nM), and SR95531 (20 μM) were added to block synaptic activity. Neurons were visualized with infrared gradient contrast microscopy (Dodt et al., 2002). Patch electrodes (Schott 8250 glass, 2–3 MΩ tip resistance, <10 MΩ series resistance) were filled with an intracellular solution containing (in mM): 113 K-Gluconate, 9 HEPES, 4.5 $MgCl_2$, 0.1 EGTA, 14 $Tris_2$-phosphocreatine, 4 Na_2-ATP, 0.3 tris-GTP; ~290 mOsm, pH: 7.22. Internal solution was supplemented with Ca^{2+}- and Na^+-sensitive dyes as described below. Dyes were allowed to equilibrate >15 min before linescans were performed. Electrophysiological data were recorded at 50 kHz and filtered at 10 kHz using a Multiclamp 700B amplifier (Molecular Devices, Sunnyvale, CA), and acquired with an ITC-18 interface (Instrutech, Port Washington, NY) using custom software written in Igor Pro (Wavemetrics, Lake Oswego, OR; software: DE Feldman). V_m was held <−75 mV with constant current injection. Action potentials were evoked via somatic depolarization (e.g., simple spikes: 1–2 nA for 2 ms), often followed by hyperpolarizing steps to prevent complex spike generation (2–400 pA for 10 ms). Data were corrected for a measured junction potential of 12 mV.

Two-photon imaging

A Ti:sapphire pulsed laser (Chameleon Ultra II; Coherent, Auburn, CA) powered a Prairie Technologies Ultima two-photon imaging system (Middleton, WI). Laser intensity was modulated with a Pockels cell (350–80 LA; Conoptics, Danbury, CT). Epi- and transfluorescence signals were captured through a 60×, 0.9 NA objective and a 1.4 NA oil immersion condenser (Olympus, Melville, NY). Fluorescence was split into red and green channels using dichroic mirrors and band-pass filters (epi: 575 DCXR, HQ525/70, HQ607/45; trans: T560LPXR, ET510/80, ET620/60; Chroma, Rockingham, VT), then focused on multialkali photomultiplier tubes (R9110; Hamamatsu, Bridgewater, NJ). Data were collected in linescan mode (2.2 ms/line, including mirror flyback). Ca^{2+} and Na^+ transient peaks were calculated from exponential fits of the fluorescence decay following stimulus offset. Unless

otherwise noted, dendritic linescans were made across processes >30 μm from the center of the soma, where the process width was relatively constant.

Ca^{2+} imaging

EGTA was omitted from the internal solution and replaced with the Ca^{2+} sensor Fluo-5F (250 μM, green) and a volume marker Alexa 594 (20 μM, red). The laser was tuned to 810 nm. Data are presented as averages of 20–40 events per site, and expressed as $\Delta(G/R)/(G/R)_{max}$*100, where $(G/R)_{max}$ was the maximal fluorescence in saturating Ca^{2+} (2 mM; Yasuda et al., 2004). $[Ca^{2+}]$ was estimated assuming a K_D of 585 nM for Fluo-5F (Brenowitz and Regehr, 2007).

Na^+ imaging

500 μM CoroNa green (stock: 50 mM in DMSO, final [DMSO]: 1%) and 20 μM Alexa 594 were added to the internal, and the laser was tuned to 810 nm. Data are presented as averages of 40–80 events per site, and expressed as $\Delta(G/R)$*100. $(G/R)_{max}$ was not determined since CoroNa cannot be saturated in physiological $[Na^+]$ (Meier et al., 2006).

Simultaneous Na^+ and Ca^{2+} imaging

Experiments were performed in GIN mice (all others in ICR mice). EGTA was excluded from the internal and replaced with 500 μM CoroNa green and the red Ca^{2+} sensor X-rhod-5F (250 μM). Gross cell morphology was mapped before patching with the laser tuned to 970 nm. The laser was re-tuned to 770 nm for Na^+/Ca^{2+} imaging. GFP fluorescence at 770 nm was 4% of its maximum at 970 nm, and undetectable at the laser intensities used for Na^+/Ca^{2+} imaging. Data are presented as $\Delta F/F_o$ for each channel, with F_o defined as fluorescence levels 0–400 ms before stimulus onset.

Pharmacology

Ca^{2+} channel blockers were bath applied (recirculation volume: 20–30 mL). Bovine serum albumin (0.1 mg/mL) was added to the Ringer before introducing drugs to minimize nonspecific peptide binding. Drugs were allowed to equilibrate for >15 min before data collection. Bath concentrations (in μM): 3 mibefradil, 0.15 Ω-agatoxin-TK, 10 nifedipine, 3 ω-conotoxin-GVIA, 0.5 SNX-482, 50 Ni^{2+}, 0.1 apamin, 0.1 iberiotoxin.

Voltage-clamp isolation of T-channel currents

Internal solution contained (in mM): 110 $CsMeSO_3$, 40 HEPES, 1 KCl, 4 NaCl, 4 Mg-ATP, 10 Na-phosphocreatine, 0.4 Na_2-GTP, 0.5 Fluo-5F, 0.02 Alexa-594; ~290 mOsm, pH: 7.22, voltages adjusted for 10 mV junction potential. Cartwheel cells were identified based on morphology, and AIS linescans were made 9.4 ± 1.2 μm from the axon hillock. T-channels were activated with voltage steps from −100 to −60 mV. Leak currents were subtracted using the P/4 protocol (Bezanilla and Armstrong, 1977) with +10 mV steps from −80 mV. Experiments were performed in the presence of 500 nM TTX, 20 μM SR95531, 500 nM strychnine, 10 mM DNQX, and 2.4 mM external Ca^{2+}.

Local mibefradil puffing

Internal solution was the same as in Ca^{2+} imaging experiments. A theta pipette (tip diameter <1 μm) was filled on one side with a vehicle solution plus 10 μM Alexa 594, and on the other side with vehicle plus 100 μM mibefradil. Vehicle solution contained (in mM): 142 NaCl, 3 KCl, 1.0 $CaCl_2$, 2.7 $MgSO_4$, 1.2 KH_2PO_4, 10 Na-HEPES, 10 glucose; pH: 7.2, ~305 mOsm. Chambers were sealed with epoxy and coupled to a single channel Picospritzer (Pressure System IIe, Toohey Co, Fairfield NJ) via a switch. The puff pipette was placed within 2 μm

of a neurite, 10–12 μm from the hillock or dendritic origin. A control complex spike was followed 2s later by a complex spike paired with a puff (2 psi, 50–100 ms duration, offset 10 ms before somatic current injection). These pairs of complex spikes were evoked every 45s. Comparisons were made between pairs, and then averaged across trials (>10 trails/condition). Spike timing was defined as the time of the peak of the action potential, and threshold V_m was defined as the maximum of the 3rd derivative before action potential peak (Henze and Buzsaki, 2001). Spike threshold was not calculated for the 3rd spikelet because it often lacked a clear threshold inflection.

Local Ni^{2+} iontophoresis

Internal solution was the same as in Ca^{2+} imaging experiments. KH_2PO_4 was removed from the Ringer to prevent $Ni_3(PO_4)_2$ precipitation (KCl was increased by 1.2 mM). A borosilicate pipette (15 MΩ tip resistance, −4 to −6 nA backing current) containing 1 M $NiCl_2$ and 50 μM Alexa 594 in water was placed close to the axon, 10 μm from the hillock. Ni^{2+} iontophoretic pulses were paired with somatic depolarization (100–200 nA, 25–40 ms, offset 5–10 ms before somatic depolarization) and interleaved with control pulses as described above. Ni^{2+} pulses had no effect on baseline G/R levels. In some experiments, an EPSP-like current injection based on the kinetics of parallel fiber-evoked EPSPs was used as described previously (Roberts et al., 2008) according to the function:

$$EPSP(t) = Amp\left(1 - e^{-t/\tau_{rise}}\right)\left(e^{-t/\tau_{decay}}\right)$$

where *Amp* was the peak EPSP amplitude (0.5–5 nA), τ_{rise} = 0.3 ms, and τ_{decay} = 1.59 ms. Ni^{2+}-induced changes in subthreshold depolarizations were considered significant when the difference between control and Ni^{2+}-paired stimuli (Ctrl-Ni^{2+}) was greater than 2 × standard deviation of the baseline voltage, 0–5 ms before stimulus onset.

Pyramidal and Purkinje cell experiments

For pyramidal cell experiments, oblique slices (300 μm thick, P17-18 ICR mice) containing one barrel in layer 4 from each whisker row were made through primary somatosensory cortex, 50° from the midsagittal plane (“across row” slices, Bender et al., 2003). For Purkinje cell experiments, parasagittal slices containing cerebellar vermi were made (300 μm thick, P14 ICR mouse). Chilled cutting/storage solution contained (in mM): 87 NaCl, 25 $NaHCO_3$, 25 glucose, 75 sucrose, 2.5 KCl, 1.25 NaH_2PO_4, 7 $MgCl_2$. Following cutting, slices were incubated for 30 min at 32 °C, then at room temperature until use. Layer 5b pyramidal cells within the whisker barrel subfield were identified based on their morphology, ability to fire spike bursts, and laminar position. For cortical experiments, DNQX, but not strychnine or SR-95531, was added to the bath. All other procedures were as in cartwheel cell experiments.

Chemicals

CoroNa green, Fluo-5F pentapotassium salt, X-rhod-5F tripotassium salt, and Alexa Fluor 594 hydrazide Na^+ salt were from Invitrogen (Carlsbad, CA). TTX, strychnine, SR95531, and DNQX were from Ascent Scientific (Weston-Super-Mare, UK). ω-agatoxin-TK, ω-conotoxin-GVIA, apamin, iberiotoxin, and SNX-482 were from Peptides International (Louisville, KY). All others were from Sigma-Aldrich (St. Louis, MO).

Statistics

All data are shown as mean ± standard error (SEM). Statistical tests are noted in text (significance: $\alpha < 0.05$). ANOVAs were followed with a Fisher’s PLSD post-hoc test.

Supplementary Material

Refer to Web version on PubMed Central for supplementary material.

Acknowledgments

We are grateful to D. Chiu, J. Christie, M. Herman, Y. Kim, S. Kuo, C. Jahr, and A. Reigel for technical assistance, and to V. Bender, I. Raman, and M. Roberts for extensive discussions and comments on this manuscript. GIN mice were provided by Sascha du Lac. Supported by NIH grants DC004450 and NS028901 (LOT), NIH training grants NS007381 and DK007680, and a Tartar Trust fellowship (KJB).

References

Aizenman CD, Linden DJ. Rapid, synaptically driven increases in the intrinsic excitability of cerebellar deep nuclear neurons. Nat Neurosci 2000;3:109–111. [PubMed: 10649564]

Bean BP. The action potential in mammalian central neurons. Nat Rev Neurosci 2007;8:451–465. [PubMed: 17514198]

Bender KJ, Rangel J, Feldman DE. Development of columnar topography in the excitatory layer 4 to layer 2/3 projection in rat barrel cortex. J Neurosci 2003;23:8759–8770. [PubMed: 14507976]

Berkefeld H, Sailer CA, Bildl W, Rohde V, Thumfart JO, Eble S, Klugbauer N, Reisinger E, Bischofberger J, Oliver D, et al. BKCa-Cav channel complexes mediate rapid and localized Ca2+-activated K+ signaling. Science 2006;314:615–620. [PubMed: 17068255]

Bezanilla F, Armstrong CM. Inactivation of the sodium channel. I. Sodium current experiments. J Gen Physiol 1977;70:549–566. [PubMed: 591911]

Bischofberger J, Geiger JR, Jonas P. Timing and efficacy of Ca2+ channel activation in hippocampal mossy fiber boutons. J Neurosci 2002;22:10593–10602. [PubMed: 12486151]

Boiko T, Van Wart A, Caldwell JH, Levinson SR, Trimmer JS, Matthews G. Functional specialization of the axon initial segment by isoform-specific sodium channel targeting. J Neurosci 2003;23:2306–2313. [PubMed: 12657689]

Brenowitz SD, Regehr WG. Reliability and heterogeneity of calcium signaling at single presynaptic boutons of cerebellar granule cells. J Neurosci 2007;27:7888–7898. [PubMed: 17652580]

Callewaert G, Eilers J, Konnerth A. Axonal calcium entry during fast 'sodium' action potentials in rat cerebellar Purkinje neurones. J Physiol 1996;495(Pt 3):641–647. [PubMed: 8887772]

Catterall WA. Localization of sodium channels in cultured neural cells. J Neurosci 1981;1:777–783. [PubMed: 6286901]

Catterall WA, Perez-Reyes E, Snutch TP, Striessnig J. International Union of Pharmacology. XLVIII. Nomenclature and structure-function relationships of voltage-gated calcium channels. Pharmacol Rev 2005;57:411–425. [PubMed: 16382099]

Cavelier P, Lohof AM, Lonchamp E, Beekenkamp H, Mariani J, Bossu JL. Participation of low-threshold Ca2+ spike in the Purkinje cells complex spike. Neuroreport 2008;19:299–303. [PubMed: 18303570]

Coombs JS, Curtis DR, Eccles JC. The interpretation of spike potentials of motoneurones. J Physiol 1957;139:198–231. [PubMed: 13492209]

Cueni L, Canepari M, Lujan R, Emmenegger Y, Watanabe M, Bond CT, Franken P, Adelman JP, Luthi A. T-type Ca2+ channels, SK2 channels and SERCAs gate sleep-related oscillations in thalamic dendrites. Nat Neurosci 2008;11:683–692. [PubMed: 18488023]

Davie JT, Clark BA, Hausser M. The origin of the complex spike in cerebellar Purkinje cells. J Neurosci 2008;28:7599–7609. [PubMed: 18650337]

Davis KA, Young ED. Granule cell activation of complex-spiking neurons in dorsal cochlear nucleus. J Neurosci 1997;17:6798–6806. [PubMed: 9254690]

Day NC, Shaw PJ, McCormack AL, Craig PJ, Smith W, Beattie R, Williams TL, Ellis SB, Ince PG, Harpold MM, et al. Distribution of alpha 1A, alpha 1B and alpha 1E voltage-dependent calcium channel subunits in the human hippocampus and parahippocampal gyrus. Neuroscience 1996;71:1013–1024. [PubMed: 8684604]

Destexhe A, Neubig M, Ulrich D, Huguenard J. Dendritic low-threshold calcium currents in thalamic relay cells. J Neurosci 1998;18:3574–3588. [PubMed: 9570789]

Dodt HU, Eder M, Schierloh A, Zieglgansberger W. Infrared-guided laser stimulation of neurons in brain slices. Sci STKE 2002;2002:PL2. [PubMed: 11854538]

Geiger JR, Jonas P. Dynamic control of presynaptic Ca(2+) inflow by fast-inactivating K(+) channels in hippocampal mossy fiber boutons. Neuron 2000;28:927–939. [PubMed: 11163277]

Goldberg EM, Clark BD, Zagha E, Nahmani M, Erisir A, Rudy B. K+ channels at the axon initial segment dampen near-threshold excitability of neocortical fast-spiking GABAergic interneurons. Neuron 2008;58:387–400. [PubMed: 18466749]

Goldberg JH, Lacefield CO, Yuste R. Global dendritic calcium spikes in mouse layer 5 low threshold spiking interneurones: implications for control of pyramidal cell bursting. J Physiol 2004;558:465–478. [PubMed: 15146046]

Harris KD, Hirase H, Leinekugel X, Henze DA, Buzsaki G. Temporal interaction between single spikes and complex spike bursts in hippocampal pyramidal cells. Neuron 2001;32:141–149. [PubMed: 11604145]

Henze DA, Buzsaki G. Action potential threshold of hippocampal pyramidal cells in vivo is increased by recent spiking activity. Neuroscience 2001;105:121–130. [PubMed: 11483306]

Herzog RI, Liu C, Waxman SG, Cummins TR. Calmodulin binds to the C terminus of sodium channels Nav1.4 and Nav1.6 and differentially modulates their functional properties. J Neurosci 2003;23:8261–8270. [PubMed: 12967988]

Kampa BM, Letzkus JJ, Stuart GJ. Requirement of dendritic calcium spikes for induction of spike-timing-dependent synaptic plasticity. J Physiol 2006;574:283–290. [PubMed: 16675489]

Kampa BM, Stuart GJ. Calcium spikes in basal dendrites of layer 5 pyramidal neurons during action potential bursts. J Neurosci 2006;26:7424–7432. [PubMed: 16837590]

Khaliq ZM, Raman IM. Relative contributions of axonal and somatic Na channels to action potential initiation in cerebellar Purkinje neurons. J Neurosci 2006;26:1935–1944. [PubMed: 16481425]

Kim Y, Trussell LO. Ion channels generating complex spikes in cartwheel cells of the dorsal cochlear nucleus. J Neurophysiol 2007;97:1705–1725. [PubMed: 17289937]

Koester HJ, Johnston D. Target cell-dependent normalization of transmitter release at neocortical synapses. Science 2005;308:863–866. [PubMed: 15774725]

Koester HJ, Sakmann B. Calcium dynamics associated with action potentials in single nerve terminals of pyramidal cells in layer 2/3 of the young rat neocortex. J Physiol 529 Pt 2000;3:625–646.

Kole MH, Ilschner SU, Kampa BM, Williams SR, Ruben PC, Stuart GJ. Action potential generation requires a high sodium channel density in the axon initial segment. Nat Neurosci 2008;11:178–186. [PubMed: 18204443]

Kole MH, Letzkus JJ, Stuart GJ. Axon initial segment Kv1 channels control axonal action potential waveform and synaptic efficacy. Neuron 2007;55:633–647. [PubMed: 17698015]

Kole MH, Stuart GJ. Is action potential threshold lowest in the axon? Nat Neurosci. 2008

Krahe R, Gabbiani F. Burst firing in sensory systems. Nat Rev Neurosci 2004;5:13–23. [PubMed: 14661065]

Lasser-Ross N, Ross WN. Imaging voltage and synaptically activated sodium transients in cerebellar Purkinje cells. Proc Biol Sci 1992;247:35–39. [PubMed: 1348119]

Lee JH, Daud AN, Cribbs LL, Lacerda AE, Pereverzev A, Klockner U, Schneider T, Perez-Reyes E. Cloning and expression of a novel member of the low voltage-activated T-type calcium channel family. J Neurosci 1999;19:1912–1921. [PubMed: 10066244]

Lisman JE. Bursts as a unit of neural information: making unreliable synapses reliable. Trends Neurosci 1997;20:38–43. [PubMed: 9004418]

Luscher C, Lipp P, Luscher HR, Niggli E. Control of action potential propagation by intracellular Ca2+ in cultured rat dorsal root ganglion cells. J Physiol 1996;490(Pt 2):319–324. [PubMed: 8821131]

Magee JC, Johnston D. Characterization of single voltage-gated Na+ and Ca2+ channels in apical dendrites of rat CA1 pyramidal neurons. J Physiol 1995;487(Pt 1):67–90. [PubMed: 7473260]

Magee JC, Johnston D. A synaptically controlled, associative signal for Hebbian plasticity in hippocampal neurons. Science 1997;275:209–213. [PubMed: 8985013]

Mainen ZF, Joerges J, Huguenard JR, Sejnowski TJ. A model of spike initiation in neocortical pyramidal neurons. Neuron 1995;15:1427–1439. [PubMed: 8845165]

Martina M, Vida I, Jonas P. Distal initiation and active propagation of action potentials in interneuron dendrites. Science 2000;287:295–300. [PubMed: 10634782]

McDonough SI, Bean BP. Mibefradil inhibition of T-type calcium channels in cerebellar purkinje neurons. Mol Pharmacol 1998;54:1080–1087. [PubMed: 9855637]

McKay BE, McRory JE, Molineux ML, Hamid J, Snutch TP, Zamponi GW, Turner RW. Ca(V)3 T-type calcium channel isoforms differentially distribute to somatic and dendritic compartments in rat central neurons. Eur J Neurosci 2006;24:2581–2594. [PubMed: 17100846]

Meier SD, Kovalchuk Y, Rose CR. Properties of the new fluorescent Na+ indicator CoroNa Green: comparison with SBFI and confocal Na+ imaging. J Neurosci Methods 2006;155:251–259. [PubMed: 16488020]

Metz AE, Jarsky T, Martina M, Spruston N. R-type calcium channels contribute to after depolarization and bursting in hippocampal CA1 pyramidal neurons. J Neurosci 2005;25:5763–5773. [PubMed: 15958743]

Molitor SC, Manis PB. Dendritic Ca2+ transients evoked by action potentials in rat dorsal cochlear nucleus pyramidal and cartwheel neurons. J Neurophysiol 2003;89:2225–2237. [PubMed: 12612001]

Oertel D, Young ED. What's a cerebellar circuit doing in the auditory system? Trends Neurosci 2004;27:104–110. [PubMed: 15102490]

Oliva AA Jr, Jiang M, Lam T, Smith KL, Swann JW. Novel hippocampal interneuronal subtypes identified using transgenic mice that express green fluorescent protein in GABAergic interneurons. J Neurosci 2000;20:3354–3368. [PubMed: 10777798]

Palay SL, Sotelo C, Peters A, Orkand PM. The axon hillock and the initial segment. J Cell Biol 1968;38:193–201. [PubMed: 5691973]

Palmer LM, Stuart GJ. Site of action potential initiation in layer 5 pyramidal neurons. J Neurosci 2006;26:1854–1863. [PubMed: 16467534]

Perez-Reyes E. Molecular physiology of low-voltage-activated t-type calcium channels. Physiol Rev 2003;83:117–161. [PubMed: 12506128]

Roberts MT, Bender KJ, Trussell LO. Fidelity of complex spike-mediated synaptic transmission between inhibitory interneurons. J Neurosci 2008;28:9440–9450. [PubMed: 18799676]

Schiller J, Helmchen F, Sakmann B. Spatial profile of dendritic calcium transients evoked by action potentials in rat neocortical pyramidal neurones. J Physiol 1995;487(Pt 3):583–600. [PubMed: 8544123]

Schmolesky MT, Weber JT, De Zeeuw CI, Hansel C. The making of a complex spike: ionic composition and plasticity. Ann N Y Acad Sci 2002;978:359–390. [PubMed: 12582067]

Shu Y, Duque A, Yu Y, Haider B, McCormick DA. Properties of action-potential initiation in neocortical pyramidal cells: evidence from whole cell axon recordings. J Neurophysiol 2007;97:746–760. [PubMed: 17093120]

Stuart G, Schiller J, Sakmann B. Action potential initiation and propagation in rat neocortical pyramidal neurons. J Physiol 1997;505(Pt 3):617–632. [PubMed: 9457640]

Sugimori M, Llinas RR. Real-time imaging of calcium influx in mammalian cerebellar Purkinje cells in vitro. Proc Natl Acad Sci U S A 1990;87:5084–5088. [PubMed: 1973300]

Tottene A, Volsen S, Pietrobon D. alpha(1E) subunits form the pore of three cerebellar R-type calcium channels with different pharmacological and permeation properties. J Neurosci 2000;20:171–178. [PubMed: 10627594]

Tzounopoulos T, Kim Y, Oertel D, Trussell LO. Cell-specific, spike timing-dependent plasticities in the dorsal cochlear nucleus. Nat Neurosci 2004;7:719–725. [PubMed: 15208632]

Williams SR, Stuart GJ. Mechanisms and consequences of action potential burst firing in rat neocortical pyramidal neurons. J Physiol 1999;521(Pt 2):467–482. [PubMed: 10581316]

Wolfart J, Roeper J. Selective coupling of T-type calcium channels to SK potassium channels prevents intrinsic bursting in dopaminergic midbrain neurons. J Neurosci 2002;22:3404–3413. [PubMed: 11978817]

Wollner DA, Catterall WA. Localization of sodium channels in axon hillocks and initial segments of retinal ganglion cells. Proc Natl Acad Sci U S A 1986;83:8424–8428. [PubMed: 2430289]

Wouterlood FG, Mugnaini E. Cartwheel neurons of the dorsal cochlear nucleus: a Golgi-electron microscopic study in rat. J Comp Neurol 1984;227:136–157. [PubMed: 6088594]

Yasuda R, Nimchinsky EA, Scheuss V, Pologruto TA, Oertner TG, Sabatini BL, Svoboda K. Imaging calcium concentration dynamics in small neuronal compartments. Sci STKE 2004;2004:pl5. [PubMed: 14872098]

Zhang S, Oertel D. Cartwheel and superficial stellate cells of the dorsal cochlear nucleus of mice: intracellular recordings in slices. J Neurophysiol 1993;69:1384–1397. [PubMed: 8389821]

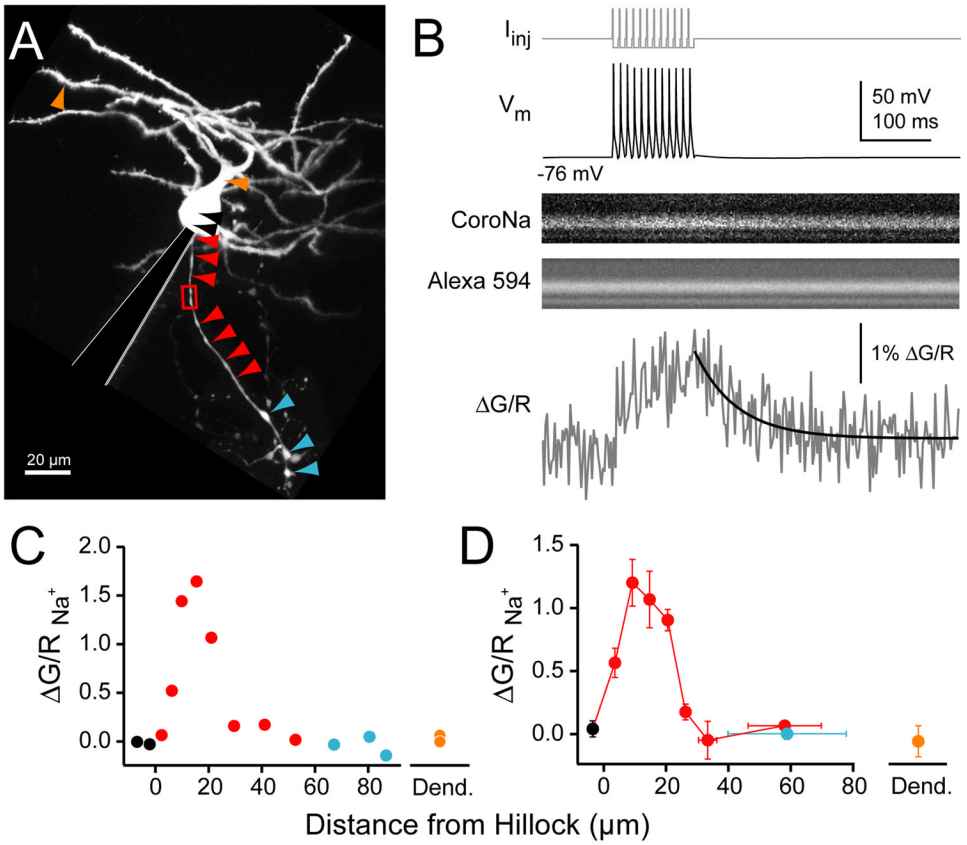

Fig. 1. Na^+ transients in cartwheel cells

(A) Maximum intensity montage of cartwheel cell. Arrowheads correspond to quantification in (C–D). Black: soma, red: axonal shaft, cyan: boutons, orange: dendrite. Red box: site of linescan highlighted in (B).

(B) Top: somatic current drives 12 simple spikes at 100 Hz. Middle: Na^+ in initial segment visualized with CoroNa, morphology visualized with Alexa 594. Bottom: Na^+ transients (grey) are computed as change in green fluorescence (G; CoroNa) over red (R; Alexa). Decay was fit with single exponential (black).

(C) Maximal ΔG/R from 100 Hz train at points shown for cell in (A).

(D) Summary ΔG/R across 4 cells (3–7 linescans/bin). Bars are SEM.

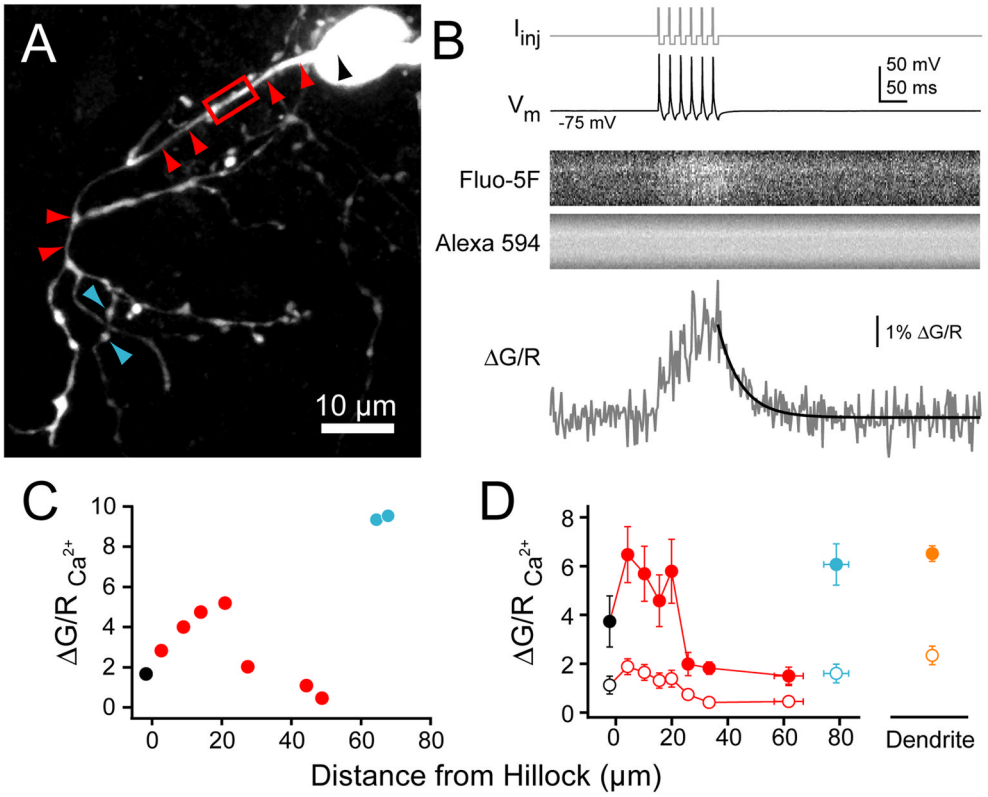

Fig. 2. Ca^{2+} transients in cartwheel cells

(A) Maximum intensity projection of cartwheel local axonal field. Arrowheads correspond to quantification in (C–D). Black: soma, red: axonal shaft, cyan: boutons. Red box: site of linescan highlighted in (B).

(B) Top: somatic current drives 6 simple spikes at 50 Hz. Middle: Ca^{2+} in initial segment visualized with Fluo-5F, morphology visualized with Alexa 594. Bottom: Ca^{2+} transients (grey) are computed as change in green fluorescence (G; Fluo-5F) over red (R; Alexa). Decay was fit with single exponential (black).

(C) Maximal ΔG/R from 50 Hz train for cell in (A) at points along axon.

(D) Summary ΔG/R across 6 cells (4–11 linescans/bin). Closed circles: 50 Hz train, open: single spikes. Linescans were performed through distal dendrite for comparison. Bars are SEM.

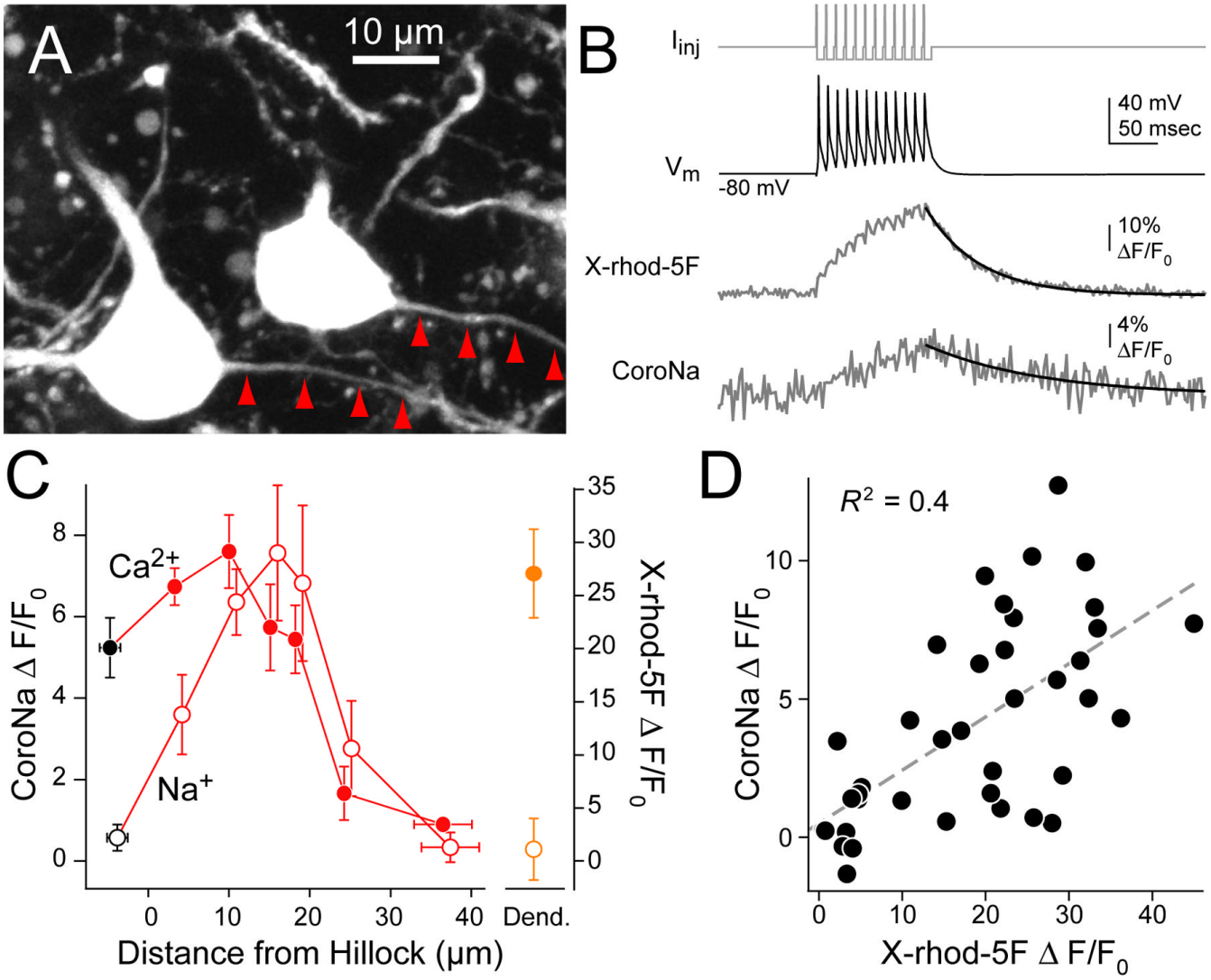

Fig. 3. Simultaneous Na^+ and Ca^{2+} imaging in GFP^+ cartwheel cells

(A) Maximum intensity projection of two GFP^+ cartwheel cells. Red arrowheads trace axons.

(B) Top: somatic current drives 12 simple spikes at 100 Hz. Bottom: example of simultaneous Ca^{2+} (X-rhod-5F) and Na^+ (CoroNa) transients 17 µm from axon hillock. Decay was fit with single exponential (black).

(C) Na^+ (CoroNa, open circles) and Ca^{2+} (X-rhod-5F, closed circles) transients in soma (black), axon (red) and dendrites (orange). Bars are SEM.

(D) Na^+ transient amplitude vs. Ca^{2+} transient amplitude at each imaging location in axon. n = 39 sites from 4 cells.

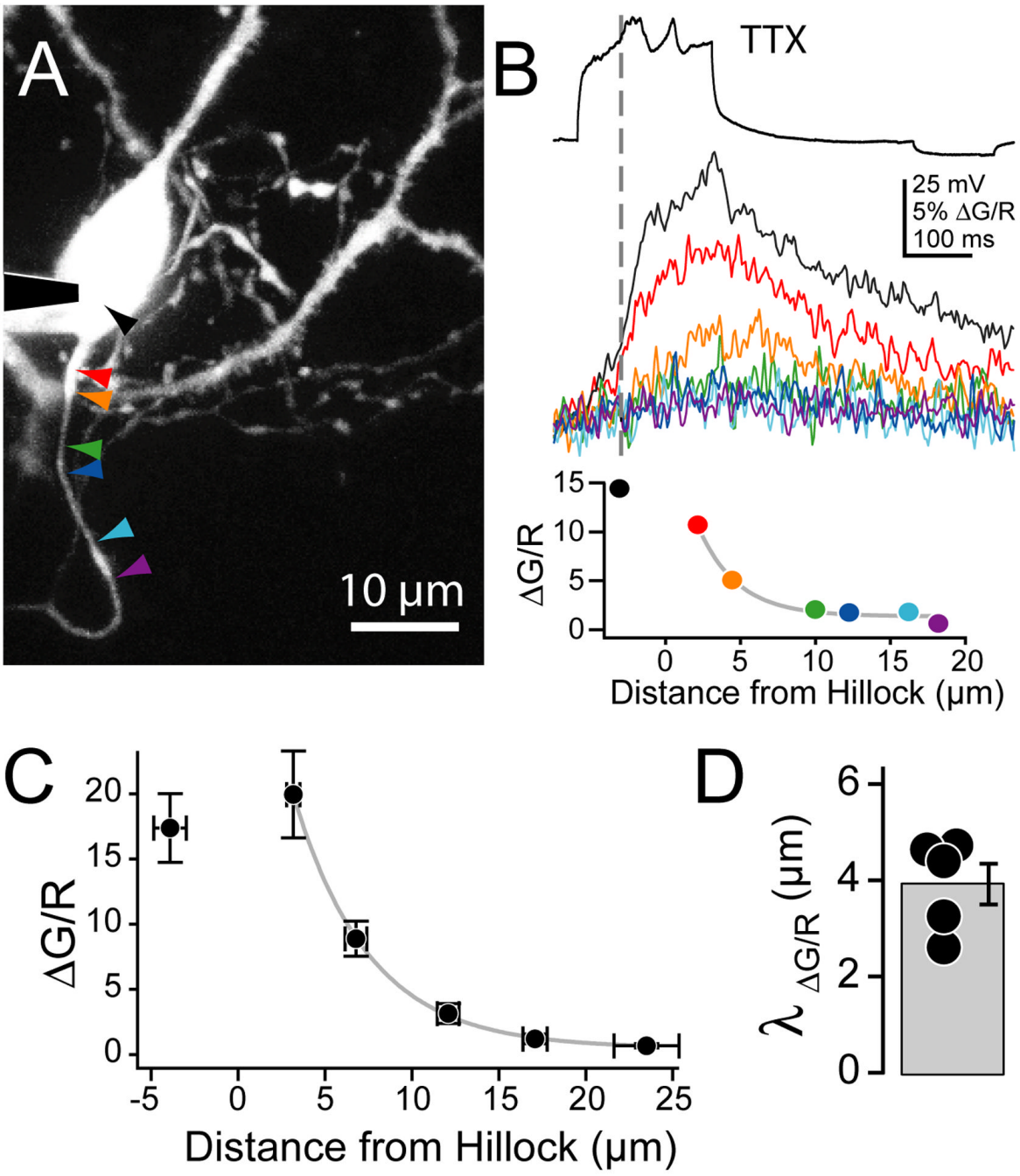

Fig. 4 . AIS Ca^{2+} requires active depolarization of the AIS

(A) Maximum intensity projection of cartwheel cell detailing axon initial segment. Arrowheads correspond to Ca^{2+} transients and peak ΔG/R amplitudes in (B) and (C), respectively.

(B) Ca^{2+} transients (middle) are aligned to the max dV/dt of initial underlying complex spike waveform isolated in 500 nM TTX (top). ΔG/R at points along axon (bottom). Colors correspond to traces above and sites in (A). Grey line: single exponential fit. Experiments performed in 2.4 mM external Ca^{2+}.

(C) Summary of decay of peak Ca^{2+} transient with distance from axon hillock (n = 5 cells).

(D) Space constant of Ca^{2+} decay. Bars are SEM.

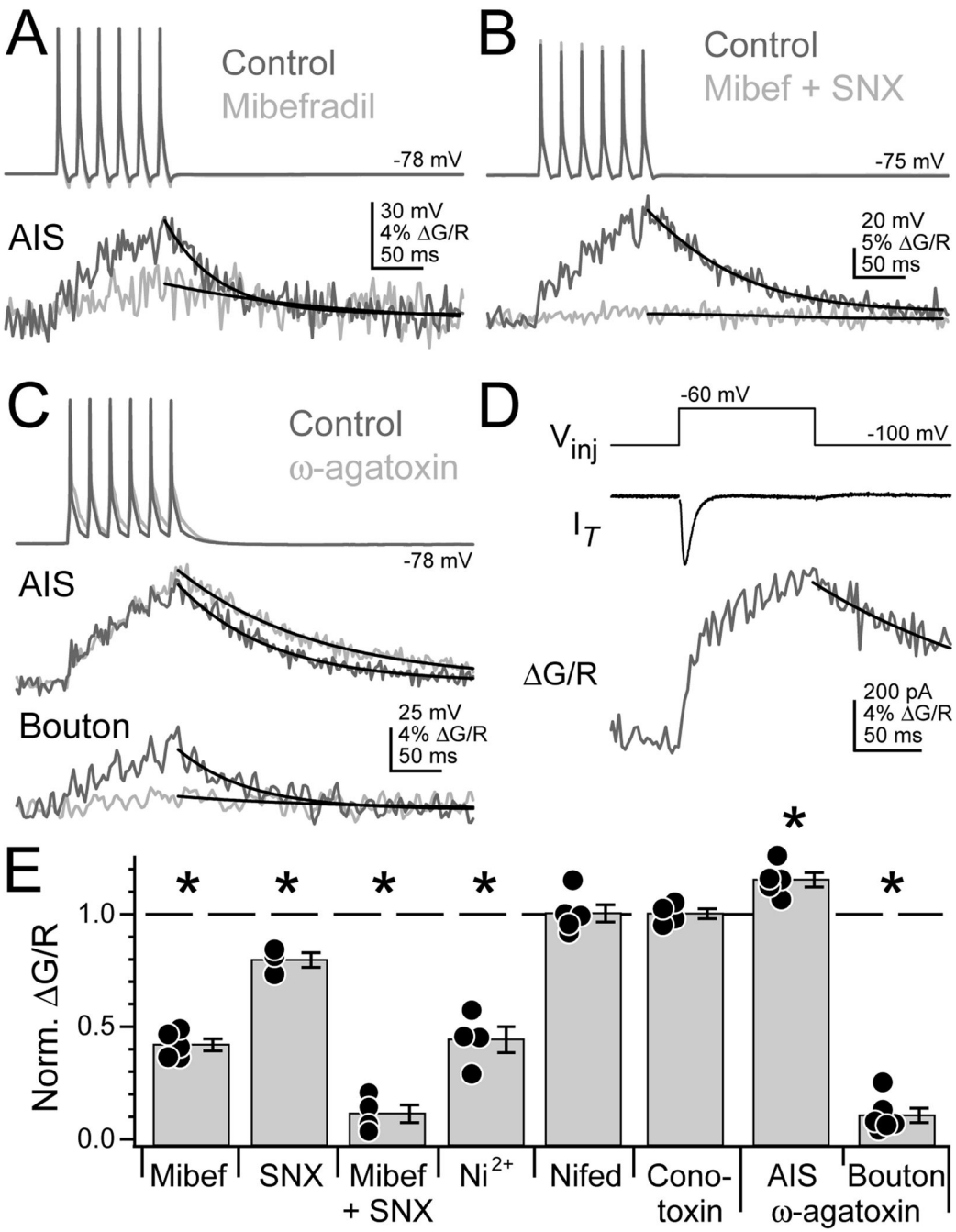

Fig. 5. AIS contains T- and R-type Ca^{2+} channels

(A) Trains of simple spikes (top) drive Ca^{2+} transients in AIS (bottom), measured 15 μm from hillock. Dark grey: control. Light grey: mibefradil in bath. Black: fits to peak.

(B) Mibefradil + SNX-482 largely abolish Ca^{2+} transient.

(C) ω-agatoxin reduces bouton Ca^{2+} transient (bottom), but not AIS Ca^{2+} (middle). Shades in (B–C) as in (A).

(D) T-channel currents (I_T, middle) isolated by voltage steps from −100 to −60 mV (top) produce a Ca^{2+} transient in AIS (bottom).

(E) Summary of Ca^{2+} transient amplitudes in the presence of various voltage-gated Ca^{2+} channel antagonists, normalized to control levels. Asterisk: $p < 0.05$, one sample t-test. Bars are SEM.

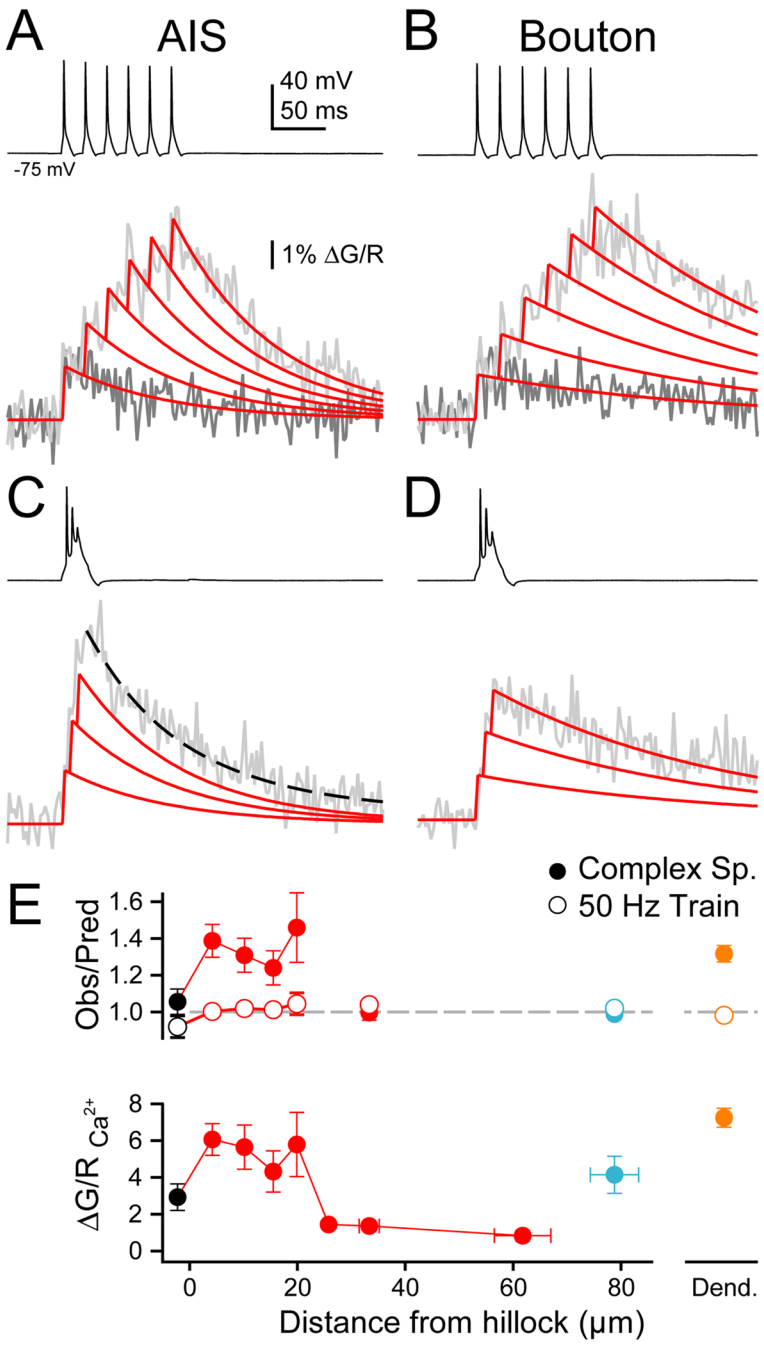

Fig. 6. Complex spike-triggered axonal Ca^{2+} transients

(A) Train (black) and corresponding Ca^{2+} imaging in AIS. Dark grey, Ca^{2+} from single spike. Light grey, Ca^{2+} from train. Red, linear sum of fit of single spike transient, temporally offset to match train timing. Scale applies to (A–D).

(B) Train in Bouton. Color code as in (A).

(C) Complex spike in AIS. Red solid: expected fit. Black dash: actual fit.

(D) Complex spike in bouton.

(E) Top, observed Ca^{2+} amplitude divided by predicted amplitude from linear sum for train and complex spike. Bottom, maximum ΔG/R values for complex spikes along axon. Color code as in Fig. 1. Bars are SEM.

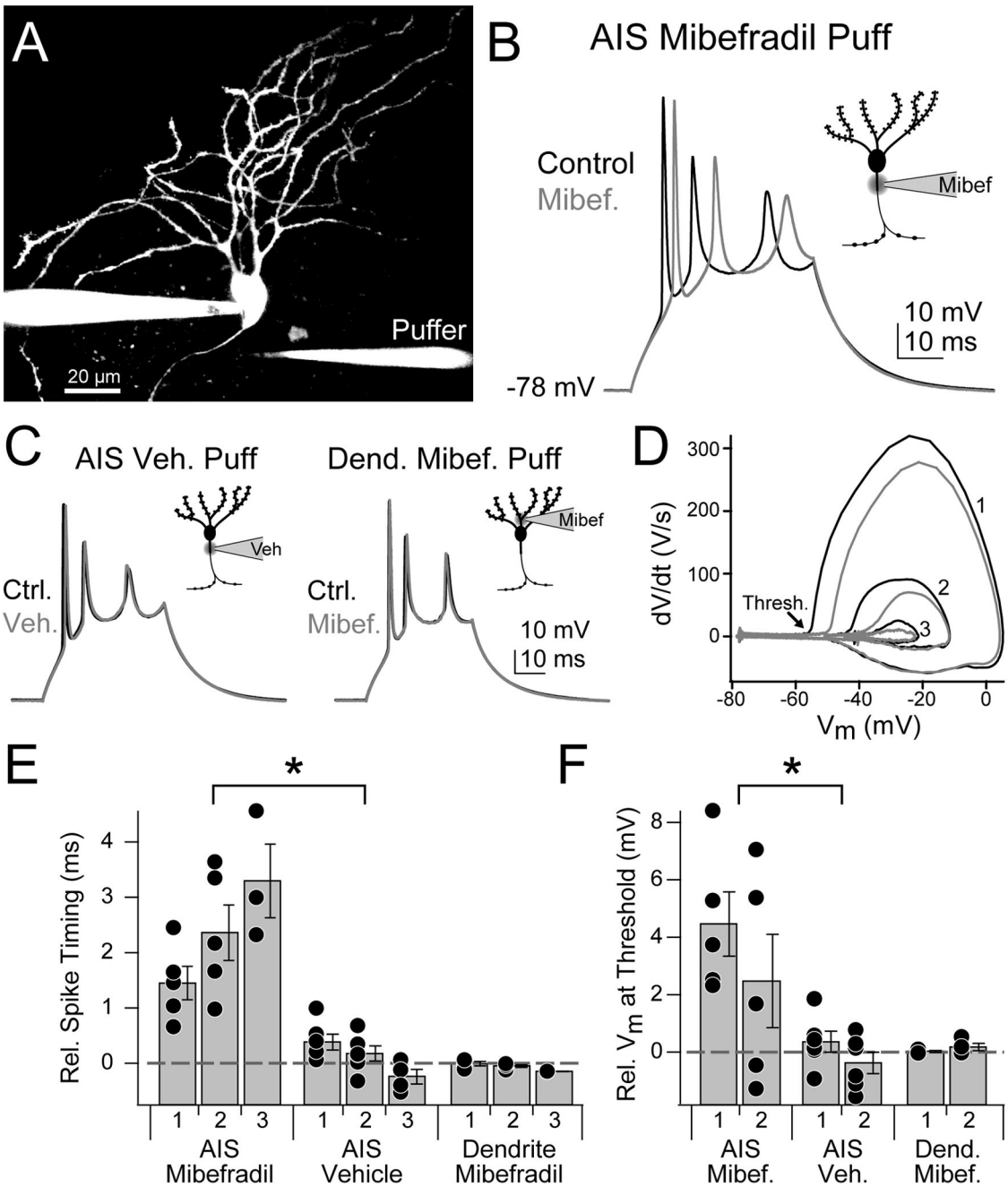

Fig. 7. AIS T-type channels shape complex spikes

(A) Maximum intensity projection of cartwheel cell showing placement of puffer pipette near AIS.

(B) Complex spikes evoked via somatic depolarization paired with mibefradil puffs onto AIS.

(C) Vehicle puffs onto AIS (left) and mibefradil puffs onto proximal dendrite (right) did not alter complex spikes. Insets in (B–C): schematic cartwheel cell detailing pipette placement.

(D) Phase plane plot of complex spikes shown in (B). Arrow shows spike threshold for first spikelet. Numbers correspond to spikelet sequence in complex spike. Color code as in (B).

(E) Relative timing of spike peak for all conditions (n = 5 cells). AIS mibefradil puffs delay spike timing.

(F) Relative threshold V_m for spikelets 1 and 2 of complex spike (n = 5). Threshold is more depolarized with AIS mibefradil puffs. Asterisk: $p < 0.05$, ANOVA. Bars are SEM.

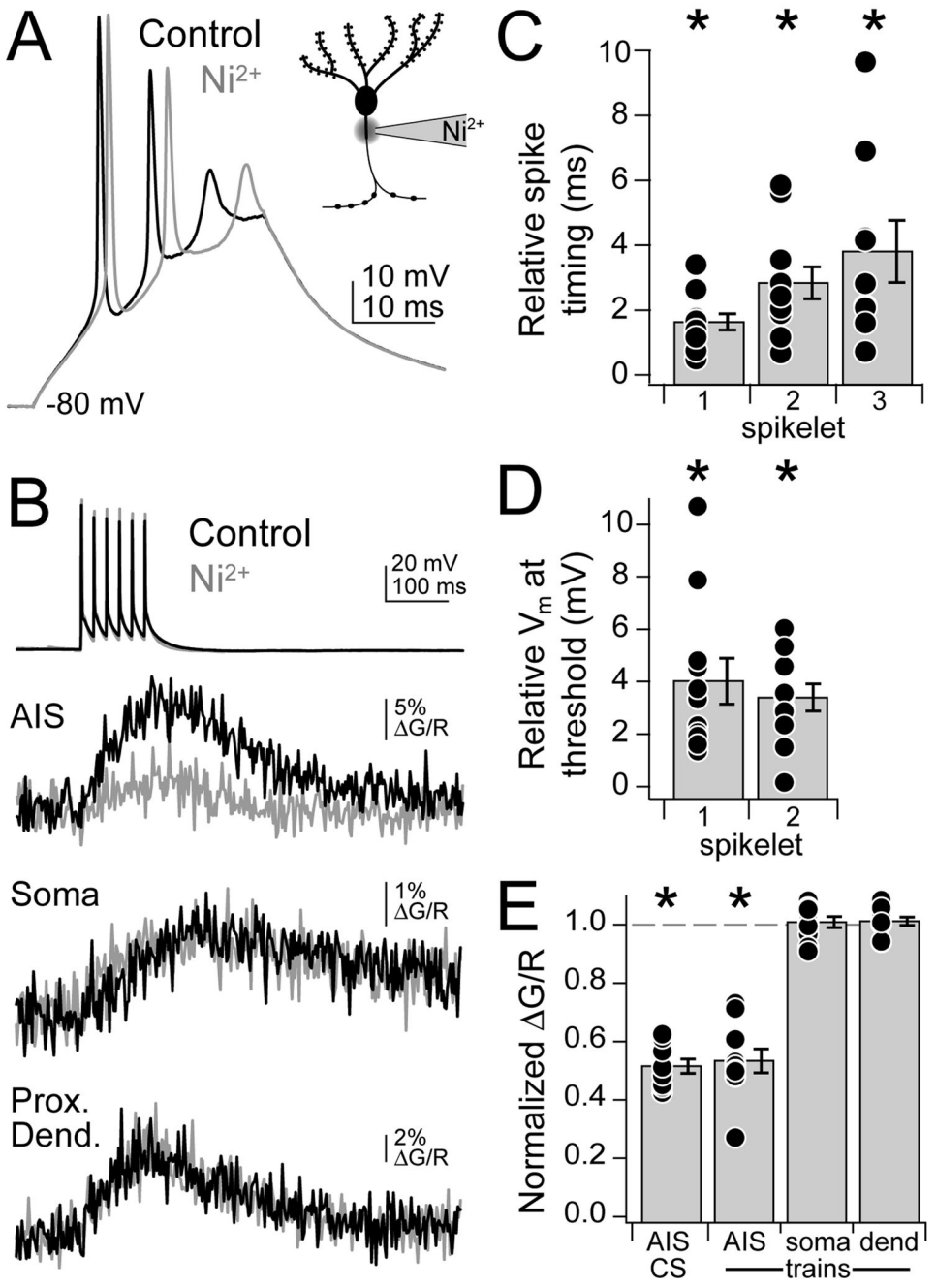

Fig. 8. AIS Ni^{2+} iontophoresis alters complex spikes

(A) Complex spikes evoked via somatic depolarization paired with Ni^{2+} iontophoresis onto AIS. Black: control. Grey: Ni^{2+}. Inset: schematic cartwheel cell detailing pipette placement.

(B) 50 Hz simple spike trains and corresponding Ca^{2+} transients in AIS, soma, and proximal dendrite in control conditions (black) and when paired with AIS Ni^{2+} iontophoretic injection (grey).

(C) Relative timing of spike peak for all conditions (n = 11 cells). Ni^{2+} delays spike timing.

(D) Relative threshold V_m for spikelets 1 and 2 of complex spike (n = 11). Threshold is more depolarized with Ni^{2+}.

(E) Normalized ΔG/R for Ni^{2+} iontophoresis compared to control conditions (n = 10). Relative amplitudes are shown for complex spikes (CS) in the AIS, and trains in the AIS, soma, and proximal dendrite. Asterisk: $p < 0.05$, one sample t-test. Bars are SEM.

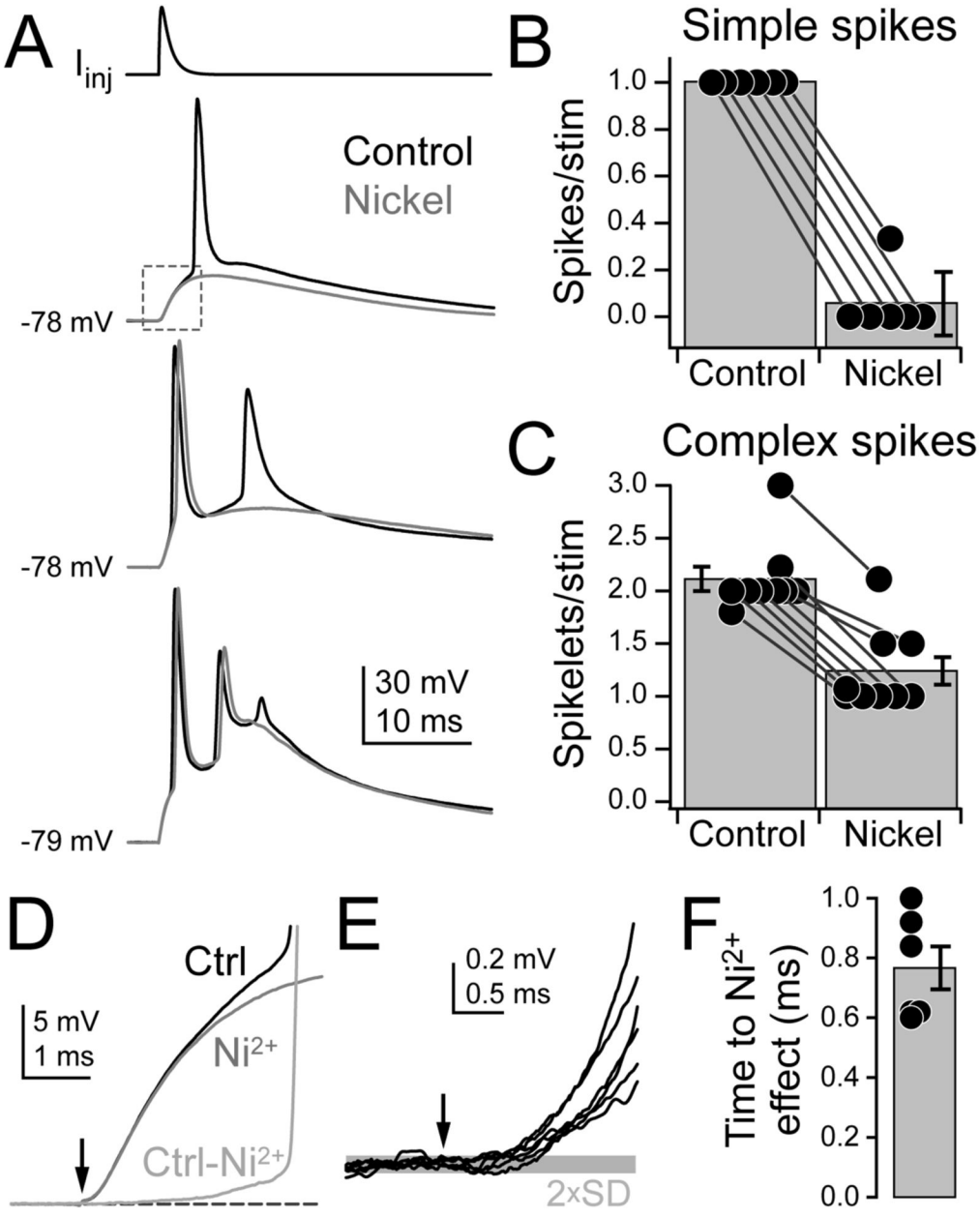

Fig. 9. AIS T-channel block reduces the probability of spiking

(A) EPSP-like injected waveform (top) of variable amplitude drives 1, 2, or 3 spikes (bottom, black). Interleaved trials paired with Ni^{2+} iontophoresis show reduced numbers of spikes (grey).

(B–C) Summary for experiments where single simple spikes (B) or complex spikes (C) were evoked. Dots are averages from 9–16 trails/cell (n = 6 simple, 9 complex). Lines connect conditions within a cell.

(D) View of area highlighted by dashed box in (A). "Ctrl-Ni^{2+}" is a subtraction of the two traces.

(E) Lines are average Ctrl-Ni^{2+} traces for each cell where single spikes were examined (n = 6, see Methods). Grey bar: Average 2×standard deviation (2×SD) of baseline. Arrow in (D–E): stimulus onset.

(F) Time Ctrl-Ni^{2+} trace emerged from noise (2×SD), relative to stimulus onset (n = 6). Bars are SEM.

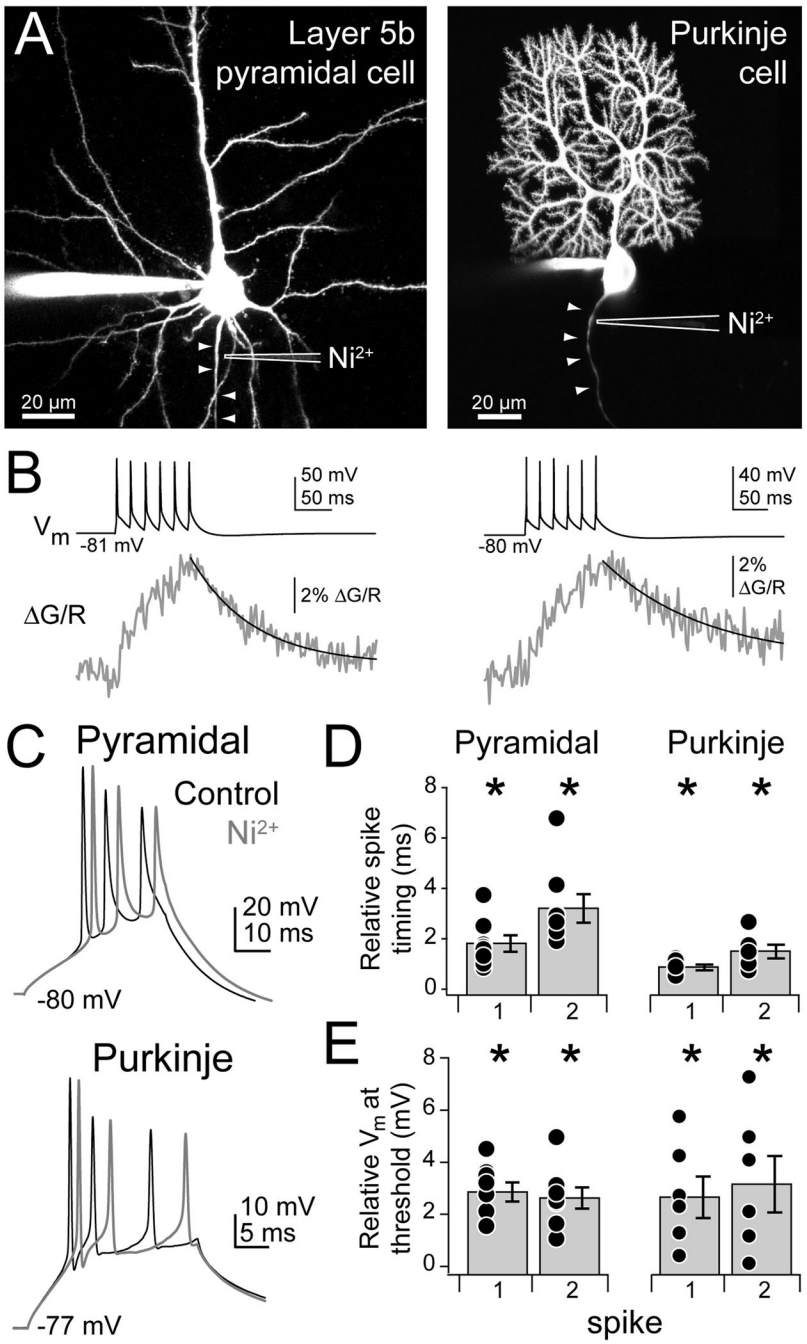

Fig. 10. AIS Ca^{2+} channels alter spike bursts in pyramidal and Purkinje cells

(A) Maximum intensity projections of cortical layer 5b pyramidal cell (left) and cerebellar Purkinje cell (right). Arrowheads follow axon. Iontophoretic pipette containing Ni^{2+} is outlined in white.

(B) Train of spikes (top) drives Ca^{2+} transients in AIS (bottom), measured 15 µm from hillock for pyramidal (left) and Purkinje cells (right).

(C) Spike bursts evoked via somatic depolarization paired with Ni^{2+} iontophoresis onto AIS in both cell types. Black: control. Grey: Ni^{2+}.

(D) Relative timing of spike peak. Ni^{2+} delays spike timing.

(E) Relative threshold V_m. Threshold is more depolarized with Ni2+. Asterisk: $p < 0.05$, one sample t-test. n = 8 pyramidal cells, 6 Purkinje cells. Bars are SEM.